

NORTHWESTERN UNIVERSITY

Equilibria as Motion Generators for Bipedal Robots

A DISSERTATION

SUBMITTED TO THE GRADUATE SCHOOL
IN PARTIAL FULFILLMENT OF THE REQUIREMENTS

for the degree

DOCTOR OF PHILOSOPHY

Field of Mechanical Engineering

By

Nelson Rosa Jr.

EVANSTON, ILLINOIS

December 2018

© Copyright by Nelson Rosa Jr. 2018
All Rights Reserved

ABSTRACT

Equilibria as Motion Generators for Bipedal Robots

Nelson Rosa Jr.

Biped robots utilize varying contact conditions and collision between their hands and feet and the walking and climbing surfaces in their environment to navigate their surroundings. This thesis presents a method for generating a continuum of gaits in a unified and extensible framework for physically-symmetric bipeds (bipeds with left and right sides that are mirror copies of each other) with point, curved, or flat feet. We detail how our framework generates open- and closed-loop walking gaits for underactuated, multi-degree-of-freedom, 2D and 3D biped walkers subject to a biped's hybrid dynamics. Specifically, we combine numerical continuation methods and virtual holonomic constraints (user-defined constrained enforced through feedback control) to generate families of gaits starting from equilibria of the biped's hybrid dynamics. In other words, we generate periodic motion from states of the biped (i.e., equilibria) that physically correspond to the biped standing still.

While equilibria themselves do not yield any net motion useful for locomoting, we show that under certain conditions that equilibria can be continuously deformed into a wide variety of walking gaits, including passive dynamic walking gaits (unactuated gaits that walk downhill under the influence of gravity) and actuated gaits that can, for example, walk on flat ground. In other words, given a parameterization of the trajectories that satisfy a biped's hybrid dynamics (the motions of the biped), we can continuously vary the value of the parameters that correspond to equilibria into values that correspond to

walking gaits. We give a sufficient condition for when equilibria can be deformed into a continuum of walking gaits and provide a computational test that reports whether the condition holds for a given biped model.

This conceptually different approach to gait generation is our main contribution to the field of bipedal locomotion. The main contribution of this thesis is the generation and analysis of a continuum of gaits for biped robots—what we call a topological approach to gait generation. Under this formulation, gaits (fixed points of a biped’s hybrid dynamics) form connected components (path-connected families of fixed points) in a space of parameterized trajectories that satisfy the biped’s hybrid dynamics.

Our topological approach is in contrast to many state-of-the-art methods that rely on formulating an optimization problem to find a single (locally) optimal gait based on a user-specified seed value with no guarantees that a gait exists near the—often randomly—chosen seed. Furthermore, it is often difficult to infer from a single gait trends and properties of a set of gaits that a continuum of gaits can afford. For example, the same hybrid dynamics that describes the motion of bipeds walking on the ground can describe the motion of brachiators swinging from treetops. Since they share similar dynamics, a well-designed walking robot might also be made to brachiate.

In this thesis, we study the connected components of a generalized two-link model that can walk and brachiate. Using our framework, we prove that previously identified compass-gait and brachiation gaits are the only two sets of limit cycles for two-link locomotors. In other words, all gaits in the parameter space can be continuously deformed into a walking-like gait or a (underhanded) brachiating-like gait. In addition, the generalized model allows examination of the stability, bifurcations, and routes to chaos of gaits under state-based switches (collisions occur whenever the swing “hand” or “foot” hits a pre-defined slope) and time-based switches (collisions occur after an elapsed period of time). We observe that while all state-based gaits are also time-based gaits, the switching strategy has a profound effect on the stability of open-loop gaits. The environmental feedback provided by a fixed slope “floor” or “ceiling” constraint can have a significant stabilizing effect not present in a time-based switching strategy.

Acknowledgements

I would like to thank the members of my committee, Todd, Randy, Russ, and Kevin for reviewing this work. While I wish I spent more time with each of you, the results of this thesis would not have been possible without, for example, Todd’s “epsilon trick”, Randy’s linear systems control class and guest lectures, the publications coming out of Russ’s lab, and Kevin’s guidance in refining the ideas and results of this thesis. Kevin, I will forever be indebted to you for taking me on as a student and for the many lessons you have taught me along the way.

I want to thank Paul for being the “sixth man” of my committee. Your feedback on my work and general support during the final years of my PhD are much appreciated. I want to recognize you as an honorary committee member for all that you’ve done.

I also want to thank my labmates in the Neuroscience and Robotics Lab (which includes when it was the Lab for Intelligent Mechanical Systems). There are too many people to list and little space to go into specifics, but thank you to Matt, Zack, Jian, Steve, Tsahai, and Tom in particular for making the lab such a great place to work. I also want to thank all of my undergraduate students who worked on the Gibbot project with me, including Andrew, Preston, Thomas, and Matt, who voluntarily dedicated their time and effort over a period of years to try and make the Gibbot work as an experimental system a reality.

I want to thank my family, especially my parents, brother, and sisters for all of their help and support. Juggling two kids under the age of three and a thesis is no easy task. The fact that you each took time off to travel to Chicago to help take care of the kids so that I could focus on my work means so much to me. An honorable mention goes to my wife and kids—but all kidding aside, your love and support has been a blessing throughout the years.

Table of Contents

ABSTRACT	3
Acknowledgements	5
Table of Contents	6
Chapter 1. Introduction	8
Chapter 2. Equilibria as Motion Generators for Bipedal Robots	10
2.1. Abstract	10
2.2. Introduction	10
2.3. Preliminaries	16
2.4. A Topological Approach to Gait Generation	22
2.5. Examples	32
2.6. Conclusion	48
2.7. Appendix A: Bipedes as Constrained Mechanical Systems	49
2.8. Appendix B: Extended Proofs of the Equilibrium Branches of M_0	52
Chapter 3. The Passive Dynamics of Walking and Brachiating Robots: Results on the Topology and Stability of Passive Gaits	55
3.1. Abstract	56
3.2. Introduction	56
3.3. The Hybrid Dynamics	58
3.4. Connected Components in the State-Time Space	59
3.5. Stability and Bifurcations	63
3.6. Discussion	64

Chapter 4. Stable Open-Loop Brachiation on a Vertical Wall	65
4.1. Abstract	65
4.2. Introduction	66
4.3. Gibbot Design and Operation	69
4.4. The Hybrid Dynamics	70
4.5. Passive Downhill Brachiation	77
4.6. Uphill Stable Brachiation	81
4.7. Discussion	82
Chapter 5. Conclusion	84
5.1. Future Work	84
References	87

CHAPTER 1

Introduction

In order to move around, bipeds use the collision between their hands and feet and the surfaces in the environment (e.g., the ground) to navigate their surroundings. This often gives these hybrid mechanical systems greater mobility in traversing complex terrain than their wheeled counterparts. However, generating motions for bipedal systems can be a challenge due to the changing contact constraints and collisions throughout the motion. A common task is to generate periodic motions, or gaits, as many bipeds are biologically-inspired robots.

This thesis presents a principled framework for generating gaits for underactuated biped robots. An important component of the framework is the ability to generate a continuum of gaits from a single gait (the motion template) in an appropriately defined space of biped motions using numerical continuation methods (NCMs). Specifically, we use the equilibria of a biped as motion templates to generate a continuum of walking gaits for underactuated, physically-symmetric bipeds subject to physical and virtual holonomic constraints (virtual constraints are constraints enforced through feedback control). In other words, under the right assumptions, we can hypothetically take a biped at rest, reposition its joints, and set its joint velocities so that the resulting motion, once we let go of the biped, is periodic. What makes our framework unique is that we can select a continuous sequence of initial poses and velocities such that once we let the biped go after placing it in the specified initial state, the biped would be in a walking gait every single time.

The basic idea behind this approach is that if we already have a known gait, then, under the right conditions, there exists more gaits in any neighborhood of points in the appropriately defined space of biped motions containing our known gait. This thesis

describes the concepts and algorithms necessary to generate these other gaits, which we expand on in the remaining chapters.

The rest of this thesis describes the framework and provides example systems where we can generate gaits from equilibria for biped robots. In particular Chapter 2 represents the main results and contributions of this thesis as whole. We provide our problem statement, statement of contributions, and our main results in Chapter 2. Chapters 3–4 demonstrate the types of analysis and results that can be obtained from our framework when applied to a two-link mechanical system. We then conclude the thesis in Chapter 5.

As an editor’s note, Chapters 2–4 are written as self-contained papers. In particular, Chapters 3–4 have been published in [67] and [65], respectively. Chapter 2 is unpublished. We intend to submit the paper as a journal paper submission to IEEE’s Transaction on Robotics or SAGE’s International Journal of Robotics Research. The papers are presented in reverse chronological order (and in order of importance to the thesis) with an evolving set of notation across these papers. We present the papers in their original form and have not attempted to edit the papers so that the notation is consistent across these chapters.

CHAPTER 2

Equilibria as Motion Generators for Bipedal Robots**2.1. Abstract**

This paper describes a topological approach to generating families of open- and closed-loop walking gaits for underactuated 2D and 3D biped walkers subject to configuration inequality constraints, physical holonomic constraints (e.g., closed chains), and virtual holonomic constraints (user-defined constraints enforced through feedback control). Our method constructs implicitly-defined manifolds of feasible periodic gaits within a state-time-control space that parameterizes the biped’s hybrid trajectories. Since equilibrium configurations of the biped often belong to such manifolds, we use equilibria as “templates” from which to grow the gait families. Equilibria are reliable seeds for the construction of gait families, eliminating the need for random, intuited, or bio-inspired initial guesses at feasible trajectories in an optimization framework. We demonstrate the approach on several 2D and 3D biped walkers.

2.2. Introduction

A challenging problem in bipedal locomotion is the gait-generation problem: given a model of a bipedal robot, generate periodic gaits subject to the biped’s hybrid dynamics and other constraints. We present an approach to the gait-generation problem where equilibria of the biped are used as templates to find families of gaits. Under certain conditions, these equilibria can be continuously deformed into a set of walking gaits, including passive dynamic walking gaits (unactuated gaits where a biped walks downhill under the influence of gravity) and actuated gaits that can, for example, enable a biped to walk on flat ground or uphill.

In this paper, we assume the biped is physically symmetric about its sagittal plane, and we are interested in symmetric *period-one* gaits: periodic gaits where each step by the right leg is identical and the mirror image of steps by the left leg.¹ Given the hybrid dynamics of the biped, the entire trajectory of a single step is represented by the finite-dimensional tuple $c = (x_0, \tau, \mu) \in \mathcal{S} = \mathcal{X} \times \mathbb{R} \times \mathcal{M}$, where $x_0 = (q_0, \dot{q}_0) \in \mathcal{X} \subseteq \mathbb{R}^{2n}$ is the initial state of the biped with configuration $q \in \mathcal{Q} \subseteq \mathbb{R}^n$; $\tau \in \mathbb{R}$ is the duration of the step; and $\mu \in \mathcal{M} \subseteq \mathbb{R}^k$ describes design or control parameters, such as k polynomial coefficients describing feedback-control-enforced coupling between joints of the biped. Our goal is to find points in \mathcal{S} that correspond to period-one gaits.

To precisely define period-one gaits, we define the flow φ such that $\varphi_\mu^\tau(x_0)$ is the biped’s state after time τ using the controls μ beginning from the state x_0 . We define the coordinate-flip operator $\text{flip} : \mathcal{X} \rightarrow \mathcal{X}$ that maps a state of the biped to its symmetric state (i.e., the equivalent state when the other leg is taking a step). The flip operator satisfies $\text{flip}(\text{flip}(x_0)) = x_0$. With these definitions, a point $c = (x_0, \tau, \mu) \in \mathcal{S}$ corresponds to a period-one gait if and only if $\varphi_\mu^\tau(x_0) - \text{flip}(x_0) = 0$.

Said another way, the *periodicity map* $P : \mathcal{S} \rightarrow \mathcal{X}$ is defined as

$$P(c) = \varphi_\mu^\tau(x_0) - \text{flip}(x_0),$$

and the set of all period-one gaits, denoted \mathcal{G} , is the set of all points $c \in \mathcal{S}$ satisfying $P(c) = 0$, i.e., $\mathcal{G} = P^{-1}(0)$.

The goal of our work is not to find a single period-one gait (a single point in \mathcal{G}), but to map out a “large” continuous family of gaits $\mathcal{G}_{\text{mapped}} \subset \mathcal{G} \subset \mathcal{S}$. The set of gaits $\mathcal{G}_{\text{mapped}}$ may include walking downhill, walking uphill, and even hand-to-hand gibbon-like swinging gaits (*brachiation*) underneath a support. A long-term goal is a full topological description of \mathcal{G} for a given state-time-control space \mathcal{S} , but that is beyond the scope of this paper.

¹The approach can be extended to general period- n gaits, such as limping gaits, but in this paper we focus on period-one gaits for simplicity.

The standard approach to finding a single gait in \mathcal{G} is to formulate a non-convex optimization problem (OP) in the parameters x_0 , τ , and μ . The convergence of non-convex OPs relies critically on the initial seed value [32, 79], which is typically chosen randomly or by applying domain-specific knowledge [13, 35, 58, 79]. No general guidelines exist for generic n -degree-of-freedom bipeds.

In our framework, however, any rest state $x_{\text{eq}} = (q_{\text{eq}}, 0)$ which is also an equilibrium (i.e., $\varphi_{\mu}^t(x_{\text{eq}}) = x_{\text{eq}}$ for some μ and any $t \geq 0$) is trivially made an equilibrium “gait” $c_{\text{eq}} = (x_{\text{eq}}, \tau, \mu)$. A subset of these equilibrium gaits are period-one gaits satisfying $P(c_{\text{eq}}) = 0$ (the rest are period-two gaits, which are not considered in this paper).² The set of all such trivial, non-locomoting equilibrium period-one gaits is denoted E , a subset of \mathcal{G} . An equilibrium gait c_{eq} is often in the same connected component of \mathcal{G} as useful locomoting gaits, and this motivates the use of numerical continuation methods (NCMs) to map out this connected component starting from c_{eq} . In other words, the easy-to-find equilibria are seeds, or “templates,” which are continuously deformed to map out $\mathcal{G}_{\text{mapped}}$.

Having a continuous family of gaits $\mathcal{G}_{\text{mapped}}$, instead of one or a small number of gaits, can be useful in a number of ways. First, some high-level walking motion planners rely on low-level gait-generation modules, or a pre-computed library of gaits, that can be applied on different terrains [29, 44, 53, 70]. A gait family $\mathcal{G}_{\text{mapped}}$ constructed using our approach is a continuous version of a gait library. Second, a gait family $\mathcal{G}_{\text{mapped}}$ allows the possibility of design of control laws that drive the biped to $\mathcal{G}_{\text{mapped}}$ rather than to a single specific gait $c \in \mathcal{G}$. In general, it is easier to design a controller to stabilize a manifold than to stabilize a point. Most importantly, $\mathcal{G}_{\text{mapped}}$ provides a global view of the possible gaits of a biped robot for the given space of design and control parameters \mathcal{M} .

²For example, the folded-over equilibria of a planar two-link biped can be made into period-one equilibrium gaits for the biped, but the equilibria where the links are fully extended cannot. To see this, consider the relative position of the swing leg with respect to the stance leg after a series of steps when the links are extended. As the legs alternate between being the stance and swing leg after each step, the relative position alternates between two distinct values making the “motion” a period-two, but not a period-one, gait.

2.2.1. Statement of Contributions

This paper describes a topological approach to generating families of walking gaits for 2D and 3D underactuated biped walkers with point, curved, or flat feet that are physically symmetric about their sagittal plane. We use NCMs to map out connected components of gaits in a state-time-control space \mathcal{S} . The biped may be subject to configuration inequality constraints, physical holonomic constraints (PHCs) such as closed chains, and virtual holonomic constraints (VHCs), i.e., user-defined constraints enforced through feedback control. Our main contributions are:

- (1) **A topological approach to the gait-generation problem.** We view gaits as points in a space \mathcal{S} of parameterized trajectories, where we explore a fundamental property of the periodic orbits of a biped’s hybrid dynamics: their connectivity to each other in \mathcal{S} across variations in state, step duration, and design and control parameters.
- (2) **The use of equilibria to generate a continuum of walking gaits.** We prove that we can find families of locomoting gaits that transversally intersect a family of equilibrium gaits in E at points $c_{\text{eq}} = (x_{\text{eq}}, \tau, \mu)$ for a given fixed pair (x_{eq}, μ) . We provide an algorithm for determining the values of τ where the intersections occur.
- (3) **A framework for generating open-loop periodic motions that satisfy the full hybrid dynamics.** We address the difficult and open problem [32] of generating open-loop periodic motions for the unactuated joints of a biped robot subject to physical and virtual holonomic constraints, including when all joints are unactuated (passive dynamic walking) and when a subset of joints track parameterized trajectories.

This paper builds on our conference paper [68] and the abstract [69]. In this previous work, we introduced the concept of using continuation methods to generate gaits for bipeds, including those subject to virtual holonomic constraints. This paper extends our preliminary work in several important ways: 1) we provide a unified framework for generating gaits from equilibrium templates for 2D and 3D underactuated bipeds subect

to configuration inequality constraints and physical and virtual holonomic constraints; 2) we provide a new algorithm to find specific types of gaits with desired properties; and 3) we provide applications of the framework to finding gaits for complex 3D bipeds such as MARLO and Atlas.

2.2.2. Related Work

The use of equilibria for generating families of unactuated walking gaits can be found in past works studying simple two- and three-degree-of-freedom passive dynamic walking biped models [22, 26, 51]. The solution families of walking gaits for these biped models converge to an equilibrium gait because the solution families exhibit a vanishing step size—as the biped’s walking slope approaches flat ground, the step size of the corresponding gait becomes shorter. In the limit, as the incline approaches level ground, the state of the biped must approach an equilibrium gait [12], a “gait” with zero step size. The work in [23] explores this notion of finding periodic walking motions near equilibria for simple walking models with vanishing step sizes. The paper gives necessary conditions on the physical parameters of planar two- and three-link bipeds for walking at arbitrarily small but near-zero slopes.

We extend the work on unactuated, low-dimensional, planar bipeds with vanishing step sizes to include powered, multi-degree-of-freedom, 2D and 3D bipeds. In our previous work [65, 67, 68], we use numerical continuation methods (NCMs) [41] to generate families of open-loop walking and brachiating gaits that utilize the “natural” or full dynamics of the biped model. In particular, [68] demonstrates that equilibria of representative point-foot planar bipeds can be continuously deformed into families of passive dynamic walking gaits. We extend this body of work to include closed-loop gaits for underactuated bipeds using the hybrid zero dynamics (HZD) framework [31, 33, 78].

The HZD framework is an experimentally-validated approach [14, 35, 62] for generating stable walking gaits for underactuated bipedal robots subject to virtual constraints (constraints on the biped that are imposed using feedback control). The notion of virtual

constraints, in particular virtual *holonomic* constraints (VHCs), has been a useful concept in the design and control of bipedal walking gaits. We enforce the VHCs using an HZD controller, which can provably impose the constraints under mild conditions [78]. Alternative control schemes for enforcing a set of VHCs also exist [71].

A common application of VHCs on a bipedal system is to have a subset of joints on an underactuated robot track polynomial trajectories that evolve with respect to a function of the biped’s configuration as oppose to time. The resulting motion is then synchronized to, for example, the motion of biped’s center of mass projected onto its tranverse plane when the constraints are properly enforced through feedback control. The net effect is that the biped only moves if the center of mass moves, irrespective of time. In such a case, the trajectories are said to be self-clocking [14].

Given a biped subject to physical and virtual holonomic constraints, we generate gaits using NCMs, which originate from results in topology and differential geometry [63]. In this context, our application is similar to tracing the points on a differentiable manifold (e.g., a curve or a higher-dimensional surface) represented as a set of equations that are continuously differentiable. An application of continuation methods for generating dynamic motion sequences of animated individuals executing parkour maneveurs can be found in [46]. The parkour moves are based on a human motion database.

NCMs are also present in optimization solvers, which many gait generation libraries rely on to generate gaits. NCMs are typically used to find feasible solutions (e.g., elastic mode in SNOPT [24]) or solve a series of related optimization problems (e.g., interior-point methods [7], like IPOPT).

The standard approach to solving the gait generation problem is to formulate it as an optimization problem (OP) [6, 36, 58]. The goal is to specify the decision variables, constraints, and objective function used in the optimization in such a way that the underlying solver (usually SNOPT, IPOPT, or fmincon) can quickly and robustly converge from an arbitrary seed value [35, 58, 79]. Recent approaches use direct collocation methods as part of the problem formulation, where the biped’s equations of motion are discretized into a set of algebraic constraints using a low-order implicit Runge-Kutta scheme with

fixed step size. A comparable optimization-based framework to our work is [36]. In [36], direct collocation methods are used to generate gaits for bipeds subject to VHCs using an HZD feedback controller to enforce the VHCs.

Our use of NCMs to find gaits differs from methods in the literature that rely on OPs in that these works attempt to find the “best” gait while we use NCMs to find many gaits without having to guess an initial seed value. However, with some effort it is possible to modify OPs to generate a continuum of gaits and NCMs to find optimal gaits.

2.2.3. Paper Outline

After covering some mathematical preliminaries in Section 2.3, we describe how to generate gaits from equilibria using numerical continuation methods in Section 2.4. In addition to providing a 1D NCM for tracing curves in \mathcal{G} , Section 2.4 gives a global description of the connected component of an equilibrium gait in E , specifies how to find branches of locomoting gaits (i.e., gaits in $\mathcal{G} - E$), and describes how to search the connected component for desired gaits once a locomoting gait has been found. In Section 2.5, we give examples of generating gaits for the compass-gait walker for illustrative purposes as well as the 3D bipeds MARLO and Atlas, in order to show that our framework can be applied to 3D models. In Section 2.6, we conclude the paper and discuss future work.

2.3. Preliminaries

In this section, we specify the biped’s hybrid dynamics, give the problem statement, state assumptions, and formally define the space of parameterized trajectories \mathcal{S} , the gait space \mathcal{G} , and the connected components of \mathcal{G} .

2.3.1. The Space of Parameterized Trajectories

The *hybrid dynamics* Σ of an n -degree-of-freedom biped robot is the tuple $\Sigma = (\mathcal{X}, f, \Delta, \phi)$, where

- \mathcal{X} is the biped’s state space;

- $f(x, u) \in T\mathcal{X}$ is a vector field to model the continuous dynamics, where $u \in \mathbb{R}^{n_u}$ is the robot controls;
- $\Delta : \mathcal{X} \rightarrow \mathcal{X}$ is a jump map to model instantaneous impacts; and
- $\phi : \mathbb{R} \times \mathcal{X} \rightarrow \mathbb{R}$ is a switching function to indicate when a foot hits the ground. If $\phi(t, x) = 0$, then $t \in \mathbb{R}$ is a *switching time*, $x \in \mathcal{X}$ is a *pre-impact state*, and the foot is in contact with the ground.

Given Σ , we are interested in hybrid trajectories that correspond to a step of a biped of the form

$$(2.1) \quad x(\tau) = \varphi_\mu^\tau(x_0) = \Delta(x_0; \mu) + \int_0^\tau f(\varphi_\mu^t(x_0), u; \mu) dt,$$

where $x_0 \in \mathcal{X}$ is the pre-impact state at $t = 0$, $\varphi_\mu^\tau(x_0) \in \mathcal{X}$ is the next pre-impact state at $t = \tau \geq 0 \in \mathbb{R}$, more generally, $\varphi_\mu^t(x_0)$ is the state of the robot at time t , $\mu \in \mathcal{M}$ is a vector of input parameters, and $u(t) \in \mathbb{R}^{n_u}$ is a vector of control inputs that depend on μ . The parameters x_0 , τ , and μ define the space of parameterized trajectories.

Definition 1. A biped's *state-time-control space* \mathcal{S} is a finite-dimensional vector space $\mathcal{S} \subseteq \mathcal{X} \times \mathbb{R} \times \mathcal{M}$. A point $c \in \mathcal{S}$, where $c = (x_0, \tau, \mu)$, defines the evolution of a hybrid trajectory $x(t) \in \mathcal{X} \subseteq \mathbb{R}^n$ given input parameters $\mu \in \mathcal{M} \subseteq \mathbb{R}^k$ starting from $x_0 \in \mathcal{X}$ at switching time $t = 0$ until the next switching time $\tau \in \mathbb{R}$.

Figure 2.1 shows how the parameters of the state-time-control space \mathcal{S} can affect the motion of an n -degree-of-freedom biped robot.

Remark 1. The input parameters μ can be used to specify design parameters of the biped such as the center of mass position of a link, leg length, spring coefficients, and moment of inertia. It can also be used to define control parameters, like feedback gains, magnitude of ankle push-off force, and spline coefficients.

As defined earlier, the set of all (period-one) gaits in \mathcal{S} is defined using the periodicity map P as

$$\mathcal{G} = \{c \in \mathcal{S} : P(c) = 0\},$$

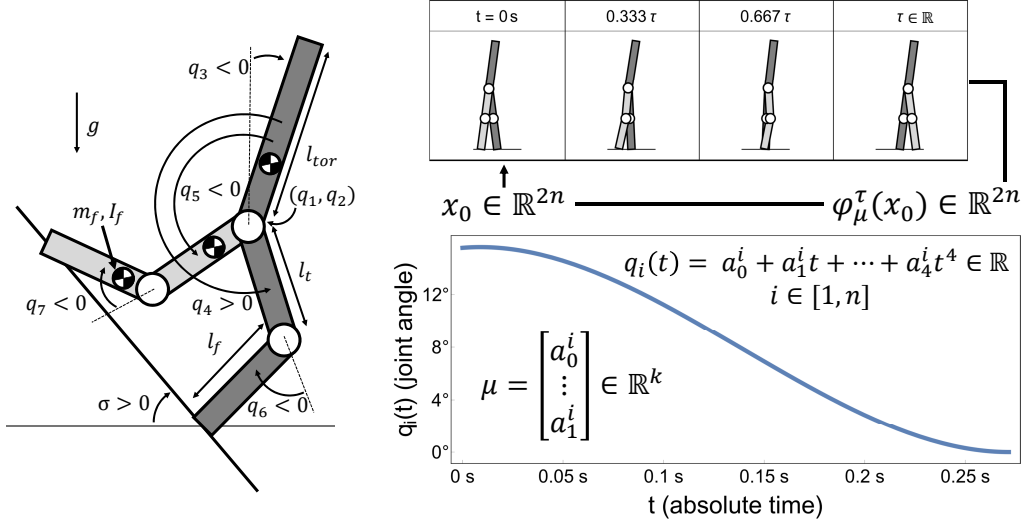


Figure 2.1. A generic n -degree-of-freedom biped model (left). We parameterize motions that satisfy the model's hybrid dynamics (top right) with a pre-impact state $x_0 \in \mathcal{X} \subseteq \mathbb{R}^{2n}$, a switching time $\tau \in \mathbb{R}$, and a vector of input parameters $\mu \in \mathcal{M} \subseteq \mathbb{R}^k$ (top and bottom right). We use the vector μ to represent any parameter that is not a state or switching time. In this example, the vector μ consists of k polynomial coefficients (bottom right) used to define the trajectory of joint q_i of the biped.

i.e., the set of all points $c = (x_0, \tau, \mu)$ satisfying $\varphi_\mu^\tau(x_0) - \text{flip}(x_0) = 0$. The set of equilibrium (stationary) gaits is defined as

$$E = \{c_{\text{eq}} = (x_{\text{eq}}, \tau, \mu) \in \mathcal{G} : f(x_{\text{eq}}, u(t); \mu) = 0 \forall t \in \mathbb{R}\},$$

i.e., the set of all points c_{eq} satisfying $P(c_{\text{eq}}) = 0$ and $\varphi_\mu^t(x_{\text{eq}}) = x_{\text{eq}}$ for all t .

2.3.2. Problem Statement

Given

- a hybrid model $\Sigma = (\mathcal{X}, f, \Delta, \phi)$ of a biped,
- a finite-dimensional space \mathcal{S} of parameterized trajectories,
- an implicit description of the set of all gaits $\mathcal{G} \subseteq \mathcal{S}$ as the points c in $P^{-1}(0)$, and

- a description of the set of equilibria $E \subset \mathcal{G}$,

use NCMs to approximately trace the connected components of \mathcal{G} that contain E . The constructed set is denoted $\mathcal{G}_{\text{mapped}}$. In cases where \mathcal{G} is more than one-dimensional, we build $\mathcal{G}_{\text{mapped}}$ recursively.

2.3.3. Assumptions

Assumption 1. Unless otherwise stated, we assume

- A1 Bipedes are physically symmetric about their sagittal plane.
- A2 Bipedes undergo exactly one collision per step, a plastic impact between the pre-impact swing leg and the ground; at impact, the pre-impact stance leg breaks contact with the ground; there is no free-flight phase (the stance leg instantaneously changes at impact); and there is no slipping at the contacts between a foot and the ground.
- A3 The next foot hits the support surface after a specified period of time has elapsed, i.e., the impact is based on time, not state.
- A4 Bipedes may be subject to physical and virtual holonomic constraints, but not nonholonomic constraints.

Assumptions A1–A2 make it so we can take advantage of a biped’s symmetry to define a gait after one step with no need for additional switching times to model other collisions during a step prior to the swing leg touching the ground again. For example, we would need additional impacts to model the knees of a walker hitting a mechanical stop to prevent hyperextension [13, 18].

Assumption A2 also states that only one foot is in contact with the ground at the time of impact making it so that only one foot is ever in contact with the ground during a step (i.e., there is no heel-toe collisions for bipeds with non-point feet [6, 36]). This is a common assumption for point- and curved-foot bipeds and one we apply to flat-footed walkers.

Assumption A3 implies that the next impact with the ground occurs after a given time, not when a state-based condition (e.g., the height of the foot above the ground drops to

zero) is satisfied. For period-one gaits, the two conditions are equivalent, however; in the time-based case, the slope of the ground is implicit, whereas in the state-based case the slope of the ground is explicit.

Given Assumption A3, the hybrid dynamics $\Sigma = (\mathcal{X}, f, \Delta, \phi)$ with fixed switching times is

$$(2.2) \quad \Sigma : \begin{cases} \dot{x}(t) = f(x(t), u(t)) & t \neq k\tau, \\ x(t^+) = \Delta(x(t^-)) & t = k\tau, \end{cases}$$

where $x(t) \in \mathcal{X}$, $f(x, u) \in T\mathcal{X}$, and $\Delta(x) \in \mathcal{X}$ are the state of the robot at time t , a vector field, and jump map, respectively (see Equation 2.1), $x(t^-)$ and $x(t^+)$ are pre- and post-impact states, respectively, and $k \geq 0 \in \mathbb{Z}$ is the k^{th} impact; the switching function ϕ is $\phi(t, x) = t - k\tau$.

Finally, Assumption A4 precludes the use of virtual nonholonomic constraints as discussed in [31]. However, a biped can be subject to n_p physical holonomic constraints (PHCs), $h_p(q) = 0 \in \mathbb{R}^{n_p}$ and n_v virtual holonomic constraints (VHCs), $h_v(q) = 0 \in \mathbb{R}^{n_v}$. The physical constraints give rise to n_p constraint forces $\lambda \in \mathbb{R}^{n_p}$. The virtual constraints are enforced using feedback control. We assume that the biped has n_u ($n_u \geq n_v$) control inputs $u(t) \in \mathbb{R}^{n_u}$ for enforcing the VHCs in the system.

2.3.4. Virtual Holonomic Constraints

Definition 2. A *phase variable* $\theta : [0, \tau] \rightarrow \mathbb{R}$ is a continuously differentiable function that is strictly monotonically increasing (or decreasing) for $t \in [0, \tau]$. If θ is strictly monotonically increasing, then the function obtains its maximum and minimum values at $\theta^+ = \theta(0^+) \in \mathbb{R}$ and $\theta^- = \theta(\tau^-) \in \mathbb{R}$, respectively.

For an n -degree-of-freedom biped with switching time τ , a VHC in this paper takes the generic form

$$(2.3) \quad q_i(t) - b_i^d(s(t), a) = 0,$$

where $q_i(t) \in \mathbb{R}$ is the joint angle ($1 \leq i \leq n$), $b_i^d(s, a) \in \mathbb{R}$ is a Bézier polynomial of degree $d \in \mathbb{N}$, $a \in \mathbb{R}^{n_a}$ is a vector of polynomial coefficients, and $s(t) \in [0, 1]$ is scaled time ($s(t) = \frac{\theta(t)}{\theta^- - \theta^+} = \frac{t}{\tau}$). We describe how to enforce a set of VHCs in Appendix 2.7.

Remark 2. The phase variable $\theta(t)$ is often a function of the biped's state [78]. However, our framework cannot generate gaits from equilibria if θ is state-based, i.e., $\theta = \theta(q(t))$. At an equilibrium point, regardless of the definition of a state-based θ , we have $\theta^+ = \theta^-$. This leads to a division by zero when we try to scale the phase variable to lie within the unit interval.

2.3.5. The Connected Components of the Gait Space \mathcal{G}

Definition 3. Let \mathcal{G} be the space of all gaits in \mathcal{S} .

- (1) A *path* between two points a and b in \mathcal{G} is a continuous function $p : [0, 1] \rightarrow \mathcal{G}$ such that $p(0) = a$ and $p(1) = b$.
- (2) A set $X \subseteq \mathcal{G}$ is *path-connected* if for all $a, b \in X$, there exists a path $p : [0, 1] \rightarrow X$ with $p(0) = a$ and $p(1) = b$.
- (3) A set $X \subseteq \mathcal{G}$ is a *connected component* of \mathcal{G} if X is path-connected and X is a maximal set with respect to inclusion.

Theorem 1. [74] Let D be an open set in \mathcal{G} , the periodicity map $P : \mathcal{S} \rightarrow \mathbb{R}^{2n}$ be a class \mathcal{C}^r differentiable function, and $P|_D : \mathcal{S} \rightarrow \mathbb{R}^{2n}$ be the restriction of P to D . If for every $c \in D$, the Jacobian $J(c) \in \mathbb{R}^{2n \times (2n+k+1)}$

$$(2.4) \quad J(c) = \frac{\partial P}{\partial c}(c) = \left[\frac{\partial \varphi}{\partial x}(c) - I_{2n}, \quad \frac{\partial \varphi}{\partial \tau}(c), \quad \frac{\partial \varphi}{\partial \mu}(c) \right]$$

has maximal rank $2n$, then D is a $(k+1)$ -dimensional (\mathcal{C}^r differentiable) manifold in \mathcal{G} .

Definition 4. A point $c \in P^{-1}(0)$ is a *singular point* of P if $\text{rank}(J(c)) < 2n$. Points are *regular* if they are not singular.

The connected components of \mathcal{G} generally consist of submanifolds of \mathcal{S} glued together at singular points of the periodicity map P . Most algorithms in this paper assume as

input a point on a differentiable manifold in \mathcal{G} , where the manifold is implicitly defined by the periodicity map P .

2.4. A Topological Approach to Gait Generation

We now present the core concepts and algorithms behind our framework. Specifically, we

- (1) describe the connected components of equilibrium gaits in the state-time-control space \mathcal{S} (Section 2.4.1),
- (2) present a continuation method for generating a path-connected set of gaits $\mathcal{G}_{\text{mapped}}$ (Section 2.4.2), and
- (3) describe how to find all paths from an equilibrium point $c_{\text{eq}} \in E \subseteq \mathcal{G}$ to a set of nonstationary gaits (nontrivial periodic orbits of the hybrid dynamics) in $\mathcal{G} - E$ given a set of switching times on a closed interval (Section 2.4.3).

The results of this section can be incorporated into other gait generation routines that want to use equilibria of a biped to generate gaits.

2.4.1. The Connected Components of Equilibrium Gaits in \mathcal{G}

Figure 2.2 is a conceptual depiction of a connected component of an equilibrium gait (EG) for an n -degree-of-freedom biped walker with one switching time and $k = 1$ design and control parameters. The dimension of \mathcal{S} is $2n + k + 1 = 2n + 2$ and the dimension of the manifolds in \mathcal{G} are $\dim(\mathcal{S}) - 2n = k + 1 = 2$ -dimensional. Examples of manifolds in the figure are the green and red-dashed curves (1D slices of a larger 2D manifold) and the green surface (a 2D manifold). The connected component has at least two singular points depicted as black dots with thick red borders.

The task is to find paths from an EG in E to a set of gaits in $\mathcal{G} - E$ on this (and other) connected components. A biped standing still is one example of an EG and in our examples of Section 2.5 is the primary EG we use to generate the gaits of $\mathcal{G}_{\text{mapped}}$ for our biped models. An EG in the gait space \mathcal{G} is always a part of a continuum of EGs of the form $(x_{\text{eq}}, \tau, \mu)$, where x_{eq} and μ are fixed and τ can take on any non-negative value

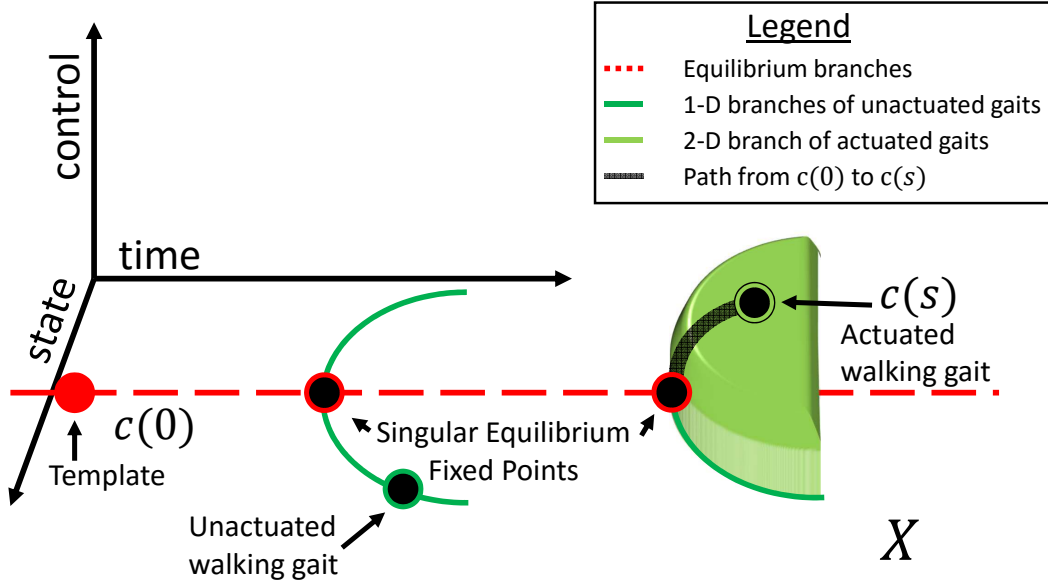


Figure 2.2. A connected component of gaits X in $P^{-1}(0)$ in the state-time-control space \mathcal{S} of a biped.

($\tau \geq 0$). A path-connected set of EGs that are regular points of the periodicity map P form an *equilibrium branch* (red dashed lines in Figure 2.2) on the connected component.

An equilibrium branch of a connected component often intersects with a branch of walking gaits. The point of intersection can only happen at EGs that are singular points of P . For example, at singular EGs in Figure 2.2, we can switch onto a non-equilibrium branch of gaits (dark green curves in Figure 2.2) and trace the branch consisting of walking gaits for inclusion into $\mathcal{G}_{\text{mapped}}$. In the next section, we give a numerical continuation method for generating these branches.

Remark 3. Equilibrium branches only exist because we assume a robot's swing foot can impact with the ground at any time. Under any state-based switching strategy, equilibria are either isolated points in \mathcal{G} or not in \mathcal{G} depending on whether conditions placed on the switching function ϕ allow for infinite impacts in zero time [3].

Algorithm 1 Pseudo-arclength Continuation Method

Require: $M : \mathbb{R}^{p+1} \rightarrow \mathbb{R}^p$, $c_0 \in M^{-1}(0)$, $\dot{c}_0 \in T_{c_0}M$, and $h \in \mathbb{R}$.

Set $c[0] = c_0$ and $\dot{c}[0] = \dot{c}_0$.

for $i := 1..N$ **do**

Prediction Step:

$$z = c[i - 1] + \dot{c}[i - 1]h$$

5: **Correction Step:**

 Solve for $M(z) = 0$ and $\dot{c}[i - 1]^T(z - c[i - 1]) = h$
 using Newton's method

Update arrays:

$$c[i] = z$$

10: Set $\dot{c}[i]$ such that $\frac{\partial M}{\partial c}(z)\dot{c}[i] = 0$ and $\|\dot{c}[i]\| = 1$

if $\dot{c}[i]^T\dot{c}[i - 1] < 0$ **then**

$$h = -h$$

end if

end for

15: **return** the solution curve c

2.4.2. Tracing Branches with Numerical Continuation Methods

Continuation methods are useful numerical tools for tracing the level set of a continuously differentiable function. While multi-parameter continuation methods exist [2, 34, 41], we present a numerical continuation method (NCM) for tracing one-dimensional manifolds, i.e., curves, $c : \mathbb{R} \rightarrow \mathcal{G}$ in the $(2n + k + 1)$ -dimensional state-time-control space \mathcal{S} . A curve in \mathcal{G} is implicitly defined such that every point on the curve $c(s) \in \mathcal{G}$ satisfies $M(c(s)) = [P(c(s))^T, \Phi(c(s))^T]^T = 0$, where $M : \mathcal{S} \rightarrow \mathbb{R}^{2n+k}$ is a continuously differentiable map, P is the periodicity map, $\Phi(c) \in \mathbb{R}^k$ is a set of k additional constraints for specifying submanifolds in \mathcal{G} to trace, and $s \in \mathbb{R}$ is the curve's arclength. The curve c is as smooth as the map M (Theorem 1).

Algorithm 1 describes the pseudo-arclength continuation method [2] for tracing a curve in \mathcal{G} using the map M . Geometrically, this algorithm defines a hyperplane a distance h away from the current point $c(s_i)$ on the curve where the search for the next point on the curve $c(s_{i+1})$ takes place; the hyperplane is normal to the tangent $\frac{dc}{ds}(s_i)$ at $c(s_i)$. The algorithm's prediction step (line 4 of the algorithm) selects a point on the plane as the initial guess using an Euler-like integration step and then a root-finding method

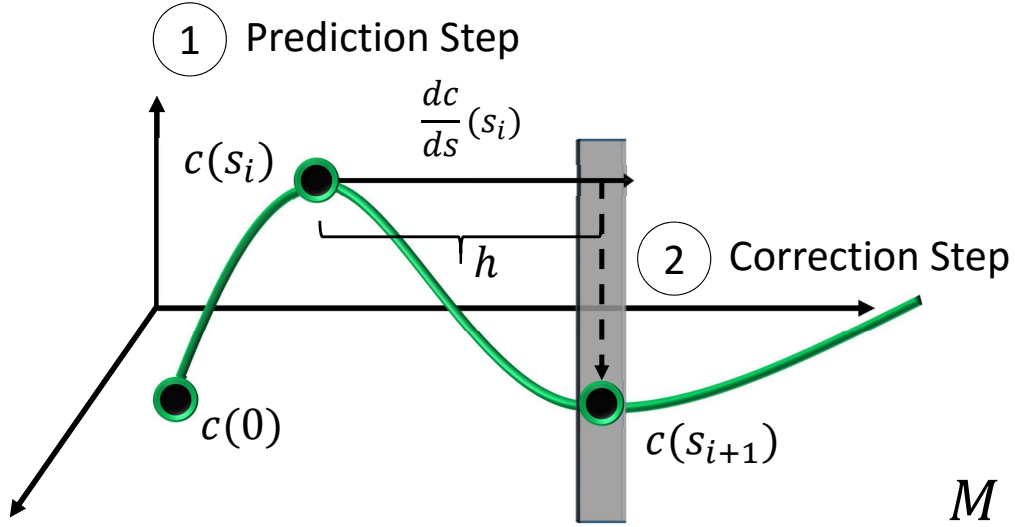


Figure 2.3. An example iteration of the pseudo-arclength continuation method as outlined in Algorithm 1.

iteratively refines the guess until the point is again back on the curve. Figure 2.3 illustrates this process.

In order to define the hyperplane, we can compute a tangent to the curve $\frac{dc}{ds}(s)$ at $c(s)$ by solving for $\frac{\partial M}{\partial c}(c(s))\frac{dc}{ds}(s) = 0$ (line 10 of Algorithm 1). In other words, the tangent $\frac{dc}{ds}(s)$ is in the null space of the Jacobian of the map M

$$(2.5) \quad T_{c(s)}M = \text{Null} \left(\frac{\partial M}{\partial c}(c(s)) \right),$$

where $T_{c(s)}M$ is the tangent space of M at $c(s)$. An arclength parameterization of the curve leads to the constraint $\|\frac{dc}{ds}(s)\| = 1$ (see [2]). If the point $c(s)$ is a regular point of M , then $\dim(T_{c(s)}M) = 1$ ($= (2n + k + 1)$ parameters minus $(2n + k)$ constraints).

Remark 4. Part of the input to Algorithm 1 is a vector $\frac{dc}{ds}(0)$ tangent to the initial point $c(0)$. If the manifold M is a one-dimensional differentiable manifold, then the tangent space is one-dimensional and there is no need to pass $\frac{dc}{ds}(0)$ as an argument; the algorithm can compute the tangent internally. However, we use NCMs to generate branches of connected components starting from a singular point, in which case, we do

need to specify the tangent vector as the null space will have dimension greater than one [2]. If we do not specify the tangent at a singular point, the behaviour of the algorithm is unknown and is implementation dependent.

With our 1D NCM, we can build the set $\mathcal{G}_{\text{mapped}}$ of higher-dimensional manifolds through multiple calls to Algorithm 1. As long as we specify a different 1D submanifold to trace on the connected component (by modifying Φ), we can continue to reuse the same EGs or any other points already in $\mathcal{G}_{\text{mapped}}$ as seed values to generate new gaits on an unexplored 1D branches of a connected component. We present an example for tracing 2D manifolds using this approach in Section 2.5.

2.4.3. Detecting Singular Equilibrium Points in the State-Time Subspace

Given the characterization of the connected components of equilibria in Section 2.4.1, we only apply Algorithm 1 after we have found a singular equilibrium gait (EG) on a connected component. We now demonstrate how to identify singular EGs in the state-time subspace. Specifically, we prove that for a given equilibrium point x_{eq} and fixed μ the indicator function

$$(2.6) \quad I(\tau) = \det \left(\frac{\partial P}{\partial x}(x_{\text{eq}}, \tau, \mu) \right),$$

when evaluated at EGs $c_{\text{eq}} \in E$ can be used to identify singular EGs. The search for a path from E to $\mathcal{G} - E$ only depends on finding switching time values of τ that make $I(\tau)$ zero. The proof requires holding the state-control subspace in \mathcal{S} fixed so that only the switching time varies.

In particular, the roots of the map $M_0 : \mathcal{S} \rightarrow \mathbb{R}^{2n+k}$

$$(2.7) \quad M_0(c) = \begin{bmatrix} P(c)^T & \Phi_0(c)^T \end{bmatrix}^T, \quad \Phi_0(c) = \mu - \mu_0,$$

where $c = (x_0, \tau, \mu) \in \mathcal{S}$ and $\mu_0 \in \mathbb{R}^k$, defines a set of curves in \mathcal{G} where every $c \in M_0^{-1}(0) \subset \mathcal{G}$ has $\mu = \mu_0 \in \mathbb{R}^k$. This constraint is enforced by the map $\Phi_0 : \mathcal{S} \rightarrow \mathbb{R}^k$. The only parameters that are allowed to vary are in the state-time subspace of \mathcal{S} . We define the sets of gaits and equilibria of M_0 as $\mathcal{G}_0 = M_0^{-1}(0)$ and $E_0 = E \cap \mathcal{G}_0$, respectively, and

Jacobian of M_0 as

$$(2.8) \quad J_0(c) = \begin{bmatrix} \frac{\partial P}{\partial c}(c) \\ \frac{\partial \Phi_0}{\partial c}(c) \end{bmatrix} = \begin{bmatrix} \frac{\partial P}{\partial x_0}(c) & \frac{\partial P}{\partial \tau}(c) & \frac{\partial P}{\partial \mu}(c) \\ 0 & 0 & I_k \end{bmatrix}.$$

Given the map M_0 , the next two propositions prove that we can find a path from an equilibrium point $c_{\text{eq}} \in E_0$ to a set of gaits in $\mathcal{G}_0 - E_0$ by searching for singular EGs in E_0 . In the first proposition, we establish the existence of 1D equilibrium branches in M_0 , which leads to a corollary that gives the condition for when an EG is a regular point in \mathcal{G}_0 .

Proposition 1. *Given*

- (1) *a biped's hybrid dynamics $\Sigma = (\mathcal{X}, f, \Delta, \phi)$,*
- (2) *an equilibrium point $x_{\text{eq}} \in \mathcal{X}$ of f ,*
- (3) *a switching time $\tau_0 \in \mathbb{R}$, and*
- (4) *a vector of input parameters $\mu_0 \in \mathbb{R}^k$*

such that $M_0(c_0) = 0$, where $c_0 = (x_{\text{eq}}, \tau_0, \mu_0) \in E_0$, if c_0 is a regular point of M_0 , then there exists a unique curve $c : (-\delta, \delta) \rightarrow E_0$ of regular points contained in E_0 that passes through c_0 at $c(0) = c_0$ for some $\delta > 0 \in \mathbb{R} \cup \{\infty\}$.

PROOF. We present the proof in Appendix 2.8. □

Corollary 1. *If $c_0 \in E_0$, then $\frac{\partial P}{\partial \tau}(c_0) = 0$ for all $c_0 \in E_0$ and $J_0(c_0)$ has rank of at most $2n + k$. Furthermore, if $c_0 \in E_0$ is a regular point of M_0 , then the submatrix*

$$\bar{J} = \begin{bmatrix} \frac{\partial P}{\partial x_0}(c_0) & \frac{\partial P}{\partial \mu}(c_0) \\ 0 & I_k \end{bmatrix} \in \mathbb{R}^{(2n+k) \times (2n+k)}$$

of the Jacobian J_0 of Equation 2.8 has full rank $2n + k$.

The next proposition states that $I(\tau)$ of Equation 2.6 can detect singular EG in E_0 .

Proposition 2. *Assume there exists a path $p : [0, 1] \rightarrow \mathcal{G}_0$ such that $p(0) \in E_0$, and $p(1) \in \mathcal{G}_0 - E_0$. If $p(0)$ is a regular point of M_0 , then*

- (1) *the path p contains at least one singular equilibrium point $p(s) \in E_0$, and*

(2) for each singular equilibrium point $p(s) \in E_0$ for $s \in (0, 1)$ the $\det(\frac{\partial P}{\partial x_0}(p(s))) = 0$.

PROOF. The proof can be found in Appendix 2.8. \square

In practice, we find that if we define a map that implicitly defines a set of one-dimensional manifolds (curves), then locally at a singular EG we find that there are only two curves that intersect each other at the singular EG. If we assume that the curves intersect transversally, then we can distinguish between the two curves with the following proposition.

Proposition 3. *Assume there exists a path $p : [0, 1] \rightarrow \mathcal{G}_0$ from $p(0) \in E_0$ to $p(1) \in \mathcal{G}_0 - E_0$ with a singular equilibrium point at $p(s_0)$ for some $s_0 \in (0, 1)$. If $\dim(T_{p(s_0)}M_0) = 2$, then there exist two curves $c_1 : \mathbb{R} \rightarrow \mathcal{G}_0$ and $c_2 : \mathbb{R} \rightarrow \mathcal{G}_0$ such that*

- (1) $M_0(c_1(s)) = M_0(c_2(s)) = 0$ for $s \in \mathbb{R}$,
- (2) $c_1(0) = c_2(0) = p(s_0)$,
- (3) $T_{p(s_0)}M_0 = \{\frac{dc_1}{ds}(0), \frac{dc_2}{ds}(0)\}$, i.e., the tangent vectors of each curve are linearly independent,
- (4) $M_0^{-1}(0)$ coincides locally with the union of the range spaces of c_1 and c_2 ,
- (5) $c_1(s) \in E_0$ for all s , and
- (6) and $c_2(s) \in \mathcal{G}_0 - E_0$ for $s \neq 0$.

PROOF. A proof of claims 1)–4) can be found in [2]. As for claims 5) and 6), we have $T_{p(s_0)}M_0 = \text{Null}(J_0(p(s_0)))$, where J_0 is the Jacobian of M_0 (Equation 2.8). Because $p(s_0)$ is a singular EG, we have from Corollary 1 and Proposition 2 that $\frac{\partial P}{\partial \tau}(p(s_0)) = 0$ and $\det(\frac{\partial P}{\partial x_0}(p(s_0))) = 0$. This implies that the null space of $J_0(p(s_0))$ has at least two linearly independent tangent vectors and, by assumption of the above proposition, it has exactly two. As $\frac{\partial P}{\partial \tau}(p(s_0)) = 0$, the Jacobian J_0 evaluated at $p(s_0)$ has the form

$$J_0(p(s_0)) = \begin{bmatrix} \frac{\partial P}{\partial x_0}(p(s_0)) & 0 & \frac{\partial P}{\partial \mu}(p(s_0)) \\ 0 & 0 & I_k \end{bmatrix}.$$

Assuming coordinates (x_0, τ, μ) , then a basis for the null space is $\text{Null}(J_0(c_0)) = \{e_0, g_0\}$, where $e_0 = [0_{2n}, 1, 0_k]^T \in \mathbb{R}^{2n+k+1}$, g_0 satisfies $g_0^T e_0 = 0$, and 0_a is a row vector of a

Algorithm 2 Detecting Singular Equilibrium Points

Require: $c_{\text{eq}} = (x_{\text{eq}}, \tau_0, \mu_0) \in E$, an interval $[a, b] \subset \mathbb{R}$, and a step size h

Define functions $c_{\text{eq}}(t) = (x_{\text{eq}}, \tau_0 + t, \mu_0)$ and

$$\delta(t) = \det \left(\frac{\partial P}{\partial x_0}(c_{\text{eq}}(t)) - I_{2n} \right)$$

$$N = \frac{b-a}{h}$$

for $i := 1..N$ **do**

$$t = a + i \times h$$

if $\delta_0(t) \times \delta_0(t-h) \leq 0$ **then**

Solve for $\delta_0(t_0) = 0$ with $t_0 \in [t-h, t]$

Store $c_{\text{eq}}(t_0)$ as a singular equilibrium point

end if

end for

return singular equilibrium points $c_{\text{eq}}(t_0)$

zeros. The tangent vector e_0 is in TE_0 . A curve $c_1(s)$ with tangent vector $\frac{dc_1}{ds}(0) = e_0$ at $c(0) = p(s_0)$ can only have points of the form $c(s) = (x_{\text{eq}}, \tau_0 + s, \mu_0)$ for $s \in [-\epsilon, \epsilon]$. The tangent vector g_0 is orthogonal to e_0 , hence curves that follow this tangent are in $\mathcal{G}_0 - E_0$. \square

Given Propositions 1–3, we can automate the search for a singular EG on a connected component using Algorithm 2. Algorithm 2 finds simple roots of Equation 2.6 (i.e., if $I(\tau) = 0$, then $\frac{dI}{d\tau}(\tau) \neq 0$) in a given interval by applying the intermediate value theorem to first bracket a root and then switch to a root-finding algorithm to accurately find the root. The step size h should be chosen with care to avoid skipping over multiple roots in a given subinterval (we use 10^{-13}). Alternative univariate root-finding algorithms can be found in [59]. In the end, all singular EGs detected on a connected component using Algorithm 2, their corresponding tangent vector(s) that are orthogonal to the switching-time dimension, and the map M_0 serve as inputs to Algorithm 1.

2.4.4. Finding Desired Gaits Using the Global Homotopy Map

The previous sections have dealt with generating gaits in the state-time subspace. In this section, we introduce a map for continuously deforming gaits found in the state-time subspace using our previous map M_0 into gaits that satisfy the periodicity constraints of

the map P and up to k additional constraints by varying all parameters (the state x_0 , switching time τ , and input parameters μ) in the state-time-control \mathcal{S} . This enables us to find gaits with desired properties, such as bipedal gait for walking on flat ground.

In a $(2n + k + 1)$ -dimensional state-time-control gait space \mathcal{S} with $2n$ periodicity constraints imposed on the space, we have branches of $(k + 1)$ -dimensional manifolds of gaits to explore on a connected component. However, we can only use Algorithm 1 to trace a one-dimensional slice of a branch at a time. If the task is to find gaits on a branch that satisfy $2n$ periodicity conditions $P(c) = 0$ with $c \in \mathcal{S}$ and up to k additional constraints, we can use the global homotopy map (GHM) [2, 39, 73] as input to Algorithm 1 in order to find gaits that satisfy the additional constraints.

The global homotopy map $G : \mathcal{G} \times \mathcal{G} \times \mathbb{R} \rightarrow \mathbb{R}^{n_h}$ is

$$(2.9) \quad G(c, a, p) = H(c) - p H(a)$$

where c and a are points in \mathcal{G} (a is considered fixed), $p \in \mathbb{R}$ is the homotopy parameter, and $H : \mathcal{S} \rightarrow \mathbb{R}^{n_h}$ is a set of n_h ($n_h \leq k$) equations whose roots we seek. These equations encode the desired gait properties we want (e.g., walk on flat ground or at a desired average velocity). The GHM obtains a root of H by starting at $(c, p) = (a, 1)$, which is a trivial root of G , and attempts to converge to a point $(c, p) = (c_0, 0)$, where c_0 satisfies $G(c_0, 0) = H(c_0) = 0$ thus making c_0 a root of H . Following [39], we eliminate the homotopy parameter p and make it a function of c and a

$$(2.10) \quad p = p(c, a) = (H(a)^T H(c)) / (H(a)^T H(a)).$$

This definition retains the properties of p at $p = 1$ and $p = 0$.

Remark 5. The GHM is a (globally convergent) generalization of the (locally convergent) Newton-Raphson root-finding method. Further background information on the GHM can be found in [2].

Let $n_G = 2n + n_h$ be the number of total constraints and $k_G = k + 1 - n_h$ be the number of expected freedoms (as singularities on a connected component can cause the number of freedoms to increase).

Given the GHM, define the map $M_a : \mathcal{G} \rightarrow \mathbb{R}^{n_G}$ as

$$(2.11) \quad M_a(c) = [P(c)^T, G(c, a, p(c, a))^T]^T$$

This map defines a k_G -dimensional manifold in \mathcal{G} that continuously deforms $a \in \mathcal{G}$ into a gait $c \in \mathcal{G}$ such that $H(c) = 0$. Thus the map enables us to find a gait c with a set of desired properties defined by the roots of H . The goal of a continuation on a branch of $M_a(c) = 0$ is to at some point in the continuation achieve $p(c, a) = 0$, if at all possible. In order to ensure sufficient progress to a root of p is being made throughout the continuation, we attempt to reduce the value of p using our one-dimensional NCM (Algorithm 1).

Proposition 4. *Let $\nabla_c p(c, a) = \frac{\partial p}{\partial c}(c, a) \in \mathbb{R}^{2n+k+1}$ and $B(s) \in \mathbb{R}^{(2n+k+1) \times k_G}$ be a matrix whose k_G columns are basis vectors for $T_c M_a$ at $c \in M_a^{-1}(0)$, where M_a is defined in Equation 2.11. Then, given a point $a \in \mathcal{G}$, selecting the tangent vector $\frac{dc}{ds}(s_i) = -B(s)B(s)^T \nabla_c p(c(s_i), a) \in T_{c(s_i)} M_a$ at every iteration i of Algorithm 1 simultaneously minimizes the function p and defines a one-dimensional curve of fixed points $c_i \in \mathcal{G}$ for $1 \leq i \leq N$.*

PROOF. We prove the proposition in two steps. First, we derive the direction of steepest descent $\Delta s \in \mathbb{R}^{k_G}$ for some parameterization $s \in \mathbb{R}^{k_G}$ of the manifold $M_a(c(s)) = 0$. We then project Δs onto the tangent space $T_c M_a$.

For the direction of steepest descent in \mathbb{R}^{k_G} , consider the optimization problem (OP):

$$(2.12) \quad \begin{aligned} & \underset{s}{\text{minimize}} && \frac{1}{2} p(c(s), a)^2 \\ & \text{subject to} && M_a(c(s)) = 0 \\ & && a \in \mathcal{G}, \end{aligned}$$

Using the method of Lagrange multipliers, the first-order optimality conditions are

$$\begin{aligned} \nabla_c p(c(s), a)^T \frac{\partial c}{\partial s}(s) + \gamma^T \frac{\partial M}{\partial c}(c(s)) \frac{\partial c}{\partial s}(s) &= 0 \\ M(c(s), a) &= 0, \end{aligned}$$

where $\gamma \in \mathbb{R}^{n_G}$ is a vector of Lagrange multipliers and $\frac{\partial c}{\partial s}(s) \in \mathbb{R}^{(2n+k+1) \times k_G}$ is a Jacobian matrix. For gaits $c(s) \in M_a^{-1}(0)$, this reduces to

$$\nabla_{c,p}(c(s), a)^T \frac{\partial c}{\partial s}(s) = \nabla_{c,p}(c(s), a)^T B(s) = 0$$

as the Jacobian of $c(s)$ must satisfy $\frac{\partial M}{\partial c}(c(s)) \frac{\partial c}{\partial s}(s) = 0$ for $c(s) \in M_a^{-1}(0)$. In other words, the original OP is an unconstrained OP when points are restricted to lie on the manifold. Hence, the steepest descent direction is $\Delta s = -B(s)^T \nabla_{c,p}(c(s), a)$ for the set of points $c(s) \in M_a^{-1}(0)$.

Algorithm 1 can be used to generate points $c(s) \in M_a^{-1}(0)$. We only need to specify a tangent vector $\frac{dc}{ds}(s) \in T_c M$ for projecting back onto M_a at every iteration. Given a basis $B(s)$ for $T_{c(s)} M_a$, we choose $\frac{dc}{ds}(s) = B(s) \Delta s$, which is a projection of the descent direction of Equation 2.12 onto the tangent space. We then arrive at $\frac{dc}{ds}(s) = B(s) B(s)^T \nabla_{c,p}(c(s), a)$, which leads to a one-dimensional curve being traced in M_a that also minimizes the homotopy parameter p . \square

In order to ensure that we are making progress towards a minimum, we can take a step of magnitude h in the direction of $\frac{dc}{ds}(s) = -B(s) B(s)^T \nabla_{c,p}(c(s), a)$ based on an Armijo line search [40].

Remark 6. This section represents a first step towards optimization on the connected components of \mathcal{G} . If we compute second-order derivatives of the hybrid dynamics, we could attempt to use a combination of first-order optimality conditions of an OP and the GHM to find optimal gaits on a manifold or use an optimization method directly (and, for gradient-based methods, project the gradient onto the manifold at each step).

2.5. Examples

We have successfully applied our framework to a representative set of bipeds taken from the literature (Figure 2.4). The biped models consist of planar passive dynamic walkers and high-degree-of-freedom actuated 3D humanoids. We have made every reasonable effort to recreate the models as presented in the literature. We do not have the space to cover each model in detail and instead focus on using equilibria to generate gaits for

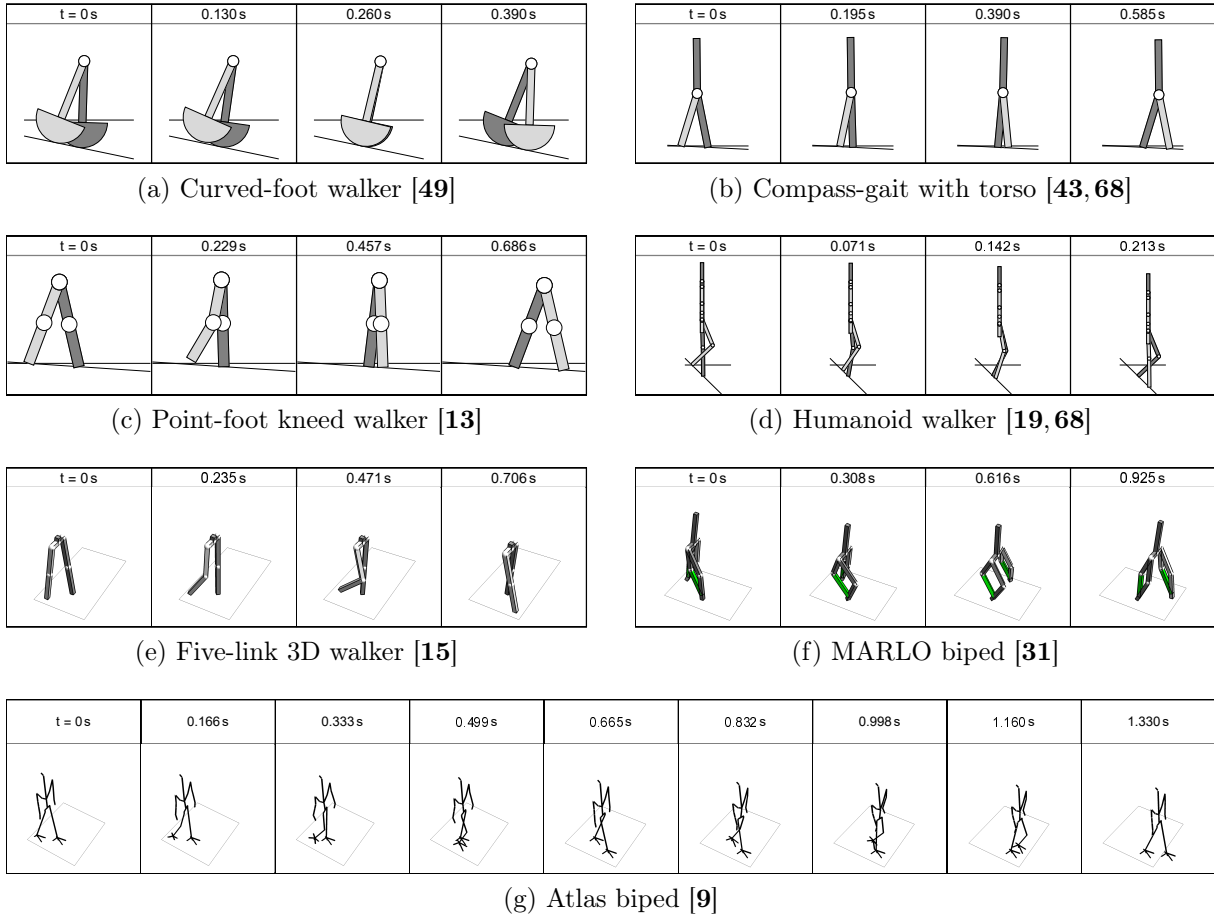


Figure 2.4. Example of period-one gaits for various planar biped walkers. The dots are joint centers. Gaits pictured in (a)-(d) are walking passively downhill and (e)-(g) are powered gaits that are subject to virtual holonomic constraints; (e)-(f) are walking on flat ground; (g) is walking downhill.

the compass-gait walker [26], MARLO biped [62] (Figure 2.4(f)), and Atlas biped [9] (Figure 2.4(g)).

For the purposes of modeling, the biped models are modeled as kinematic trees with floating bases attached to their pelvis. If the biped is planar the floating base has three configuration variables, otherwise the floating base has six configuration variables. The contact constraints between the stance foot and the ground determine the path of the

Cartesian coordinates (a subset of $\{q_x, q_y, q_z\}$) of a biped’s floating base so we often omit the Cartesian coordinates when describing the models. Unless otherwise noted,

- physical quantities are measured in SI units (i.e., meters, kilograms, seconds),
- the gaits reported in this paper have a normed error between two consecutive pre-impact states $x_0 = (q, \dot{q})$ of less than 10^{-8} (with q having units of radians and \dot{q} radians per second),
- the search window for singular equilibrium gaits (EGs) for Algorithm 2 is $\tau \in [0.1, 1]$ divided into 100 steps, and
- the step size $h \in \mathbb{R}$ of the numerical continuation method of Algorithm 1 is $-\frac{1}{20}$ and $\frac{1}{20}$ in order to trace both sides of a curve and we attempt to generate at least 50 gaits per function call.

Our general approach for generating gaits for 3D bipeds (Figure 2.4(e)–(g)) is a two-step process:

- (1) First, we generate gaits for a planar version of the biped subject to virtual holonomic constraints, if the constraints are useful or necessary.
- (2) Then, we apply a Global Homotopy Map (GHM, Section 2.4.4) to continuously deform a gait of the planar model into a gait of the 3D model.

The first step is primarily for the case where the 3D biped model does not have any equilibria from which we can start from. In other words, the biped does not have enough control authority to balance itself on one foot while at rest. The second step in our approach is straightforward, the use of the GHM enables us to search for a viable gait for the 3D biped model using a gait for a planar model as the seed value for the GHM. We provide more specifics on how we implement these steps with the actual biped models.

2.5.1. An Illustrative Example of Gait Generation using the Compass-Gait Walker

We present an example of extending equilibria to periodic orbits for the compass-gait walker [26]. The compass-gait walker is a common two-link model used to study walking gaits. The biped model (Figure 2.5(a)), walking under the influence of gravity g , consists

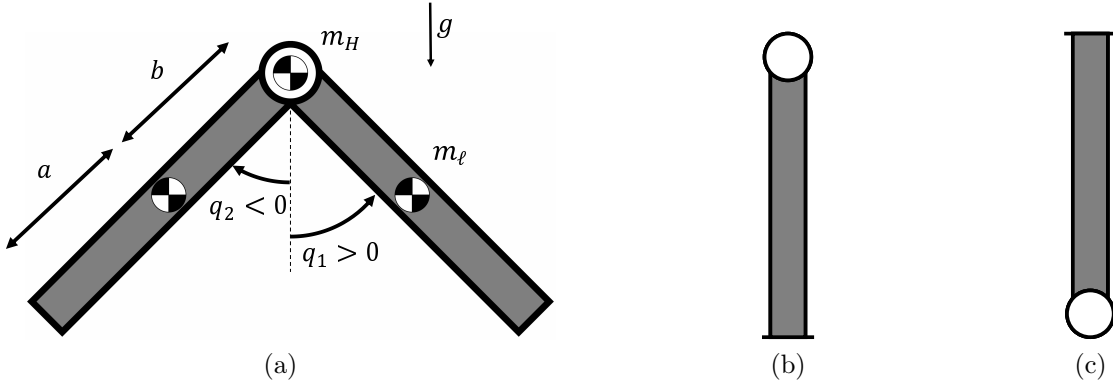


Figure 2.5. The compass-gait model and two equilibrium points in \mathcal{G} . The legs in the model have the same physical parameters a , b , and m_ℓ .

of two legs with point mass m and lengths $a + b$. The biped also has a large point mass m_H at the hip. The biped's symmetry makes the search for period-one gaits possible. We use the same values for the physical parameters as in [26] with $\frac{m_H}{m} = 2$, $\frac{b}{a} = 1$, and $g = 9.81 \text{ m/s}^2$. The state of the robot is $x = [q_1, q_2, \dot{q}_1, \dot{q}_2]^T \in \mathbb{R}^4$, representing the two leg angles and their velocities. With this minimal set of coordinates, we can directly compare our results to those in [26] using the same exact model. The angle of the walking surface $\sigma \in \mathbb{R}$ is implicitly defined according to the position of the swing leg's foot at $t = 0$, $\sigma = \frac{1}{2}(q_1(0) + q_2(0))$. The biped has no motors ($n_u = 0$), no VHCs ($n_v = 0$), and two PHCs ($n_p = 2$) representing the no-slip contact conditions between the stance foot and the ground.

After using this data to derive the biped's hybrid dynamics, the goal is to find period-one walking gaits in a five-dimensional state-time-control space \mathcal{S} . A point $c \in \mathcal{S}$ consists of the pair (x_0, τ) , where $x_0 \in \mathcal{X}$ is a pre-impact state and $\tau \in \mathbb{R}$ is a switching time (in seconds). There are no input parameters $\mu \in \mathcal{M}$ ($k = 0$). Given the five parameters that define the state-time-control space and the four periodicity constraints of the periodicity map P , we expect to find one-dimensional manifolds of gaits in \mathcal{S} . The search for a walking gait starting on a manifold of equilibrium gaits (EGs) is a three step process:

- (1) Identify a subset of EGs of interest in $E \subset \mathcal{G}$,

- (2) Choose a $c_{\text{eq}} \in E$ and use Algorithm 2 to find all singular EGs in a closed interval of switching times $\tau \in [a, b] \subset \mathbb{R}$ where $0 \leq a < b$,
- (3) Call Algorithm 1 with the map $M_0 = P$, a singular EG c_{eq} , and the correct tangent vector $\frac{dc_{\text{eq}}}{ds}(s) \in T_{c_{\text{eq}}}P$.

The first step for the compass gait is straightforward. The biped's state space \mathcal{X} has four equilibrium points (EGs), but only two EGs in \mathcal{X} correspond to fixed points of \mathcal{G} . These are $x_{\text{eq}} = [0, 0, 0, 0]^T$ and $x_{\text{eq}}^\pi = [\pi, \pi, 0, 0]^T$ (Figure 2.5(b)–(c)). These points define the set of equilibria $E \subset \mathcal{G}$, where $E = E_0 \cup E_\pi$, $E_0 = \{c_{\text{eq}} \in \mathbb{R}^5 : [0, 0, 0, 0, \tau]^T\}$, and $E_\pi = \{c_{\text{eq}} \in \mathbb{R}^5 : [\pi, \pi, 0, 0, \tau]^T\}$. We start our search using the equilibrium x_{eq} , which gives rise to nearby walking gaits. If we had started with x_{eq}^π , we would find nearby (overhand) brachiating gaits.

We next apply Algorithm 2 to find roots of the indicator function $I(\tau)$ of Equation 2.6 over the interval $\tau \in [0, 1]$. The roots correspond to the singular EGs of Figure 2.6 at $\tau = 0.62 \text{ s}$ and $\tau = 0.68 \text{ s}$, respectively.

At these singular EGs, there are two tangent vectors in the null space of $J(c) = \frac{\partial P}{\partial c}(c)$ of Equation 2.4. If the basis for the null space is orthonormal, then the tangent vector that leads to the branch of walking gaits is orthogonal to the switching-time dimension in \mathcal{S} . An orthonormal basis for the nullspace evaluated at $J(x_{\text{eq}}, 0.62)$ is

$$(2.13) \quad \{e_0, [0.13, -0.12, 0.72, 0.67, 0]^T\},$$

where $e_0 = [0, 0, 0, 0, 1]^T$ and at $J(x_{\text{eq}}, 0.68)$ is

$$(2.14) \quad \{e_0, [0.13, -0.13, 0.69, 0.69, 0]^T\}.$$

The desired tangent in each case is not e_0 (which points along the switching time dimension), as shown in the proof of Proposition 3.

As the final step, we apply the pseudo-arclength continuation method of Algorithm 1 starting from each of the singular EGs identified in the previous step. Figures 2.6–2.7 show the resulting set of gaits $\mathcal{G}_{\text{mapped}}$ and animations of a selection of gaits from $\mathcal{G}_{\text{mapped}}$, respectively.

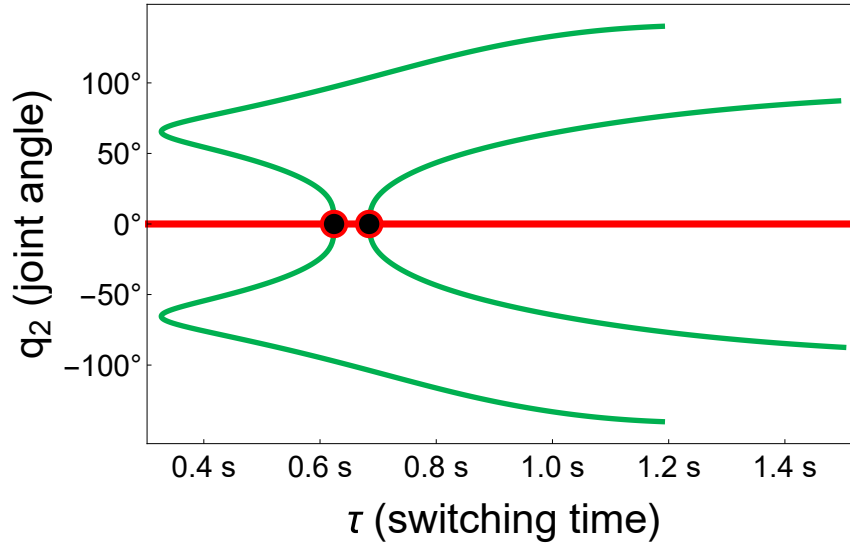
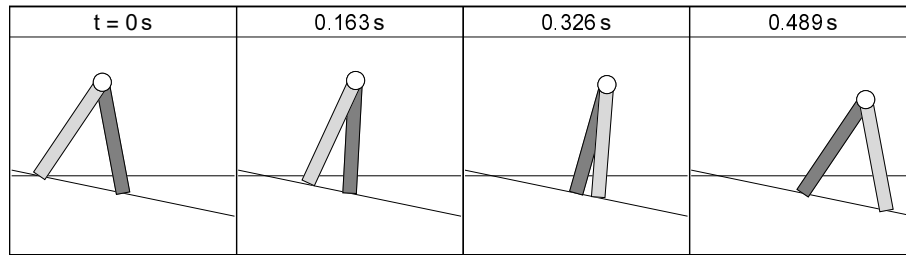


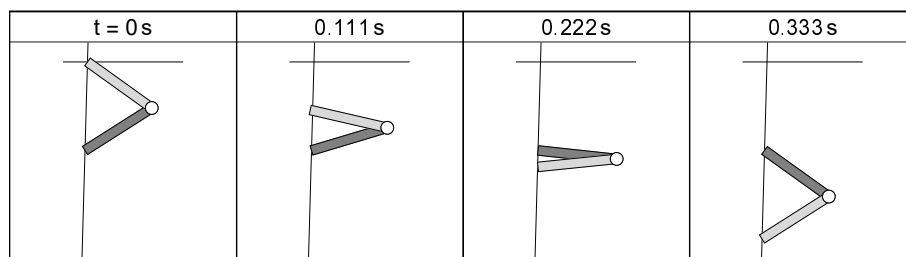
Figure 2.6. A 2D projection of a connected component of the compass gait onto a subspace of its state-time-control space \mathcal{S} . The “points of intersection” (black dots) are singular points. These points allow us to switch from an equilibrium branch (red) onto a branch with walking gaits (green).

In particular, the path-connected set of gaits in Figure 2.6 reflect the description given earlier in Section 2.4.1 of the connected components of EGs. In this plot, we have seven different 1D manifolds of gaits (red and green curves) joined together at two singular EGs (black dots). In particular, $(x_{\text{eq}}, 0)$ is part of a set of equilibrium branches of gaits with zero net displacement (red line) such that (x_{eq}, τ) is a point on these branches for all τ . The red line of EGs intersects with two green branches of walking gaits. The points of intersection at $\tau = 0.62$ s and $\tau = 0.68$ s for the compass gait correspond to the start of the “short” and “long” solution branches of walking gaits as reported in [26]. The (symmetric) green branches that extend from each singular point contain gaits that are mirror images of each other, i.e., if one branch has state x_0 , the other branch has state $-x_0$; the sign indicates whether the gait walks downhill to the left or right of its initial stance.

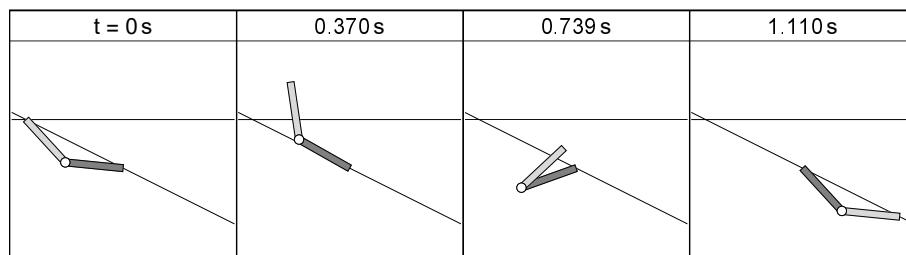
In Figure 2.7, we see the existence of gaits in $\mathcal{G}_{\text{mapped}}$ over a range of slopes that include walking and overhand brachiating gaits. Each of the gaits in Figure 2.7 can be continuously deformed into each other and are part of the same connected component of the EG $(x_{\text{eq}}, 0)$ depicted in Figure 2.5(b).



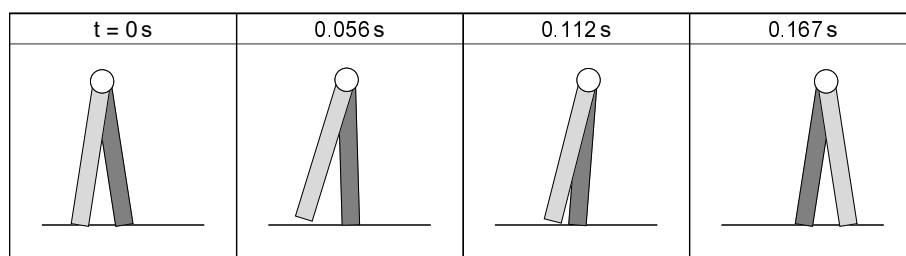
(a)



(b)



(c)



(d)

Figure 2.7. Example period-one gaits of the compass-gait walker. Gaits (a)-(c) are passive dynamic walking gaits ($u(t) = 0$ for all time t) and (d) is an actuated gait ($u(t) = \mu_0 \sin(2\pi t)$, $\mu_0 \in \mathbb{R}$) walking on flat ground.

2.5.2. Extending Passive Gaits into a Family of Actuated Gaits

If we add a motor at the hip joint of the robot, the state-time-control space \mathcal{S} can be augmented with control dimensions. In general, increasing the dimension of \mathcal{S} will also increase the dimension of \mathcal{G} , extending it into the control subspace. The original \mathcal{G} is just the slice of the extended \mathcal{G} when $\mu = 0$.

We use the motor to drive the hip with the torque $u_0(t) = \mu_0 \sin(\omega t)$ [38], where the amplitude $\mu_0 \in \mathbb{R}$ is a control parameter. The angular frequency is fixed at $\omega = 2\pi$ to keep this example low dimensional. The control subspace is now one-dimensional ($k = 1$) and we have added an actuator ($n_u = 1$) to the model. Design parameters could also be defined. For example, a parameter defining the curvature of the feet [49] or position of the center of mass [51] could be added. In this example, however, we only add the control parameter μ_0 .

In this six-dimensional state-time-control space \mathcal{S} consisting of points (x_0, τ, μ_0) , we have two-dimensional gait manifolds (the six parameters minus the four periodicity constraints). The passive gaits of the previous section are now a slice of this higher-dimensional gait space $\mathcal{G} \subset \mathbb{R}^6$, where the control parameter μ_0 is zero (Figure 2.8).

We generated the surface of Figure 2.8 by calling Algorithm 1 with two different maps as input. In the first set of calls to Algorithm 1, we use the map M_0 of Section 2.4.3 to generate a set of passive gaits using the seed values $(x_{\text{eq}}, 0.62, 0)$ and $(x_{\text{eq}}, 0.68, 0)$ (i.e., the singular points of the original \mathcal{G} space mapped to the extended \mathcal{G} space). We then use every locomoting passive dynamic walking gait found as seed values to Algorithm 1 using a second similarly defined map $M_\tau : \mathcal{S} \rightarrow \mathbb{R}^{2n+k}$, which holds τ constant and allows μ_0 to vary during the continuation.

This higher-dimensional example shows that we can grow $\mathcal{G}_{\text{mapped}}$ from an EG to a set of passive gaits to an even larger set of actuated gaits by adding extra parameters to the state-time-control space \mathcal{S} . We use this notion of growing a manifold from slices of a lower-dimensional subset of gaits on the manifold for our 3D bipeds as well. In this case, we generate gaits for a planar version of the biped and use these walking gaits to generate gaits for the 3D model.

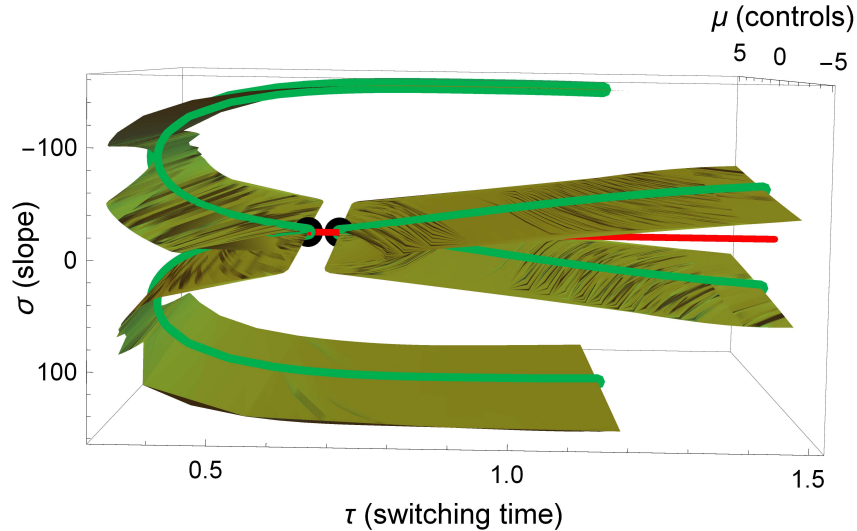


Figure 2.8. The connected component of the compass-gait walker in a higher-dimensional state-time-control space (see Figure 2.2 for legend). The curves of passive gaits in Figure 2.6 are slices of this space where $\mu_0 = 0$ (green and red curves).

2.5.3. Generating Gaits for a Flat-footed Walking Biped with Arms

We have tested our technique on a simulation of a modified version of Boston Dynamics’ Atlas robot, a 3D flat-footed walking biped (Figure 2.9(b)). The use of flat-footed walking constraints are inspired by the reduced models of [36, 58], which only considers the legs of Atlas as their biped model. In this example, we generate gaits for a biped with fewer actuators than internal degree of freedoms ($n_u < n - 6$). The goal of this example is to demonstrate that we can generate gaits for complicated bipeds subject to VHCs that are severely underactuated.

The modified biped model we use for Atlas is derived from a DARPA Robotics Challenge “.cfg” file available online [57]. This source file generates the biped’s URDF file for use in ROS and Gazebo. The only modifications we make to the model is diagonalizing the moment of inertia tensor of the pelvis, middle and upper back, and neck links. Otherwise, we use the full biped model with a 6D floating base at the pelvis. The biped walks in the x - z plane (its sagittal plane), but has dynamics in the x , y , and z coordinate directions. Gravity points in the downward z direction.

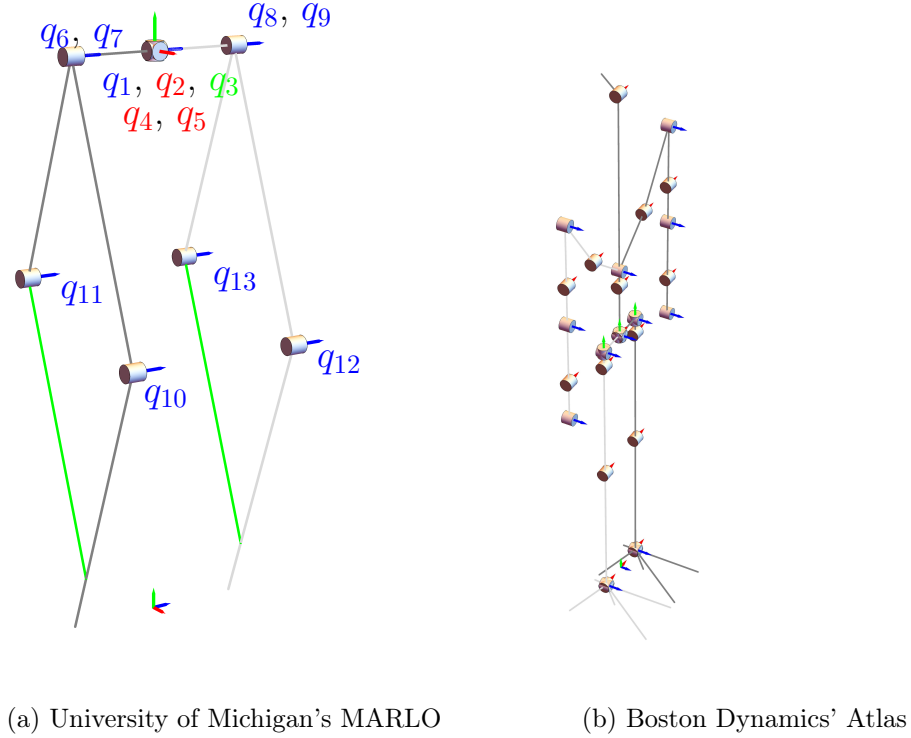


Figure 2.9. Mechanical structure and coordinates for (a) MARLO and (b) Atlas biped models. The light gray links are on the “right-side” of the bipeds, the cylinders are joints, the arrows emanating from the cylinders are the (positive) rotation axes, and the frames in-between the feet are world frames. In addition, MARLO has joint centers that overlap and are not visible, and green links to emphasize the leg’s four-bar structure.

Our model of Atlas has 34 degrees of freedom (Figure 2.9(b)), but with 6 physical holonomic constraints (PHC), 22 virtual holonomic constraints (VHCs) and actuators ($n_p = 6$, $n_u = n_v = 22$), we can define the biped’s pre-impact state $x_0 \in \mathcal{X}$ using 12 states ($n = 12$). While the biped has 22 actuators to enforce its VHCs, six of its internal joints are unactuated. Because of space constraints, we simply summarize the VHCs. The VHCs do change depending on which leg, left or right, is the stance leg.

When the right leg is the stance leg pre-impact at $t = 0^-$, the configuration and velocities of the joints that rotate about the y -axis of the hips, right shoulder, right ankle, right elbow, and right wrist joint specify x_0 . These states are unactuated and do not have

associated VHCs post-impact at $t = 0^+$ (in which case, the left leg is the stance leg). The configurations and velocities of all other joints, except the left knee joint, are subject to VHCs that force the joints to track third-order Bézier polynomials (post-impact when the left leg is the stance leg). The VHC of the left knee joint keeps the relative knee angle locked at zero degrees throughout the motion post-impact.

The boundary conditions for the Bézier polynomials for the arms subject to VHCs mirror their counterparts (e.g. $q_{\text{left elbow}}(0^-) = -q_{\text{right elbow}}(\tau^-)$ and $q_{\text{left elbow}}(\tau^-) = -q_{\text{right elbow}}(0^-)$). All other joints subject to VHCs are at rest at the beginning and end of a step.

A similar partitioning of the joints exists for when the left leg is the stance leg prior to impact and the right leg is the stance leg post-impact.

Unlike the compass-gait biped, Atlas cannot balance itself on one foot without collapsing on itself. We modify the biped’s physical parameters using three dimension-less control parameters $\omega_1, \omega_2, \omega_3 \in [0, 1]$ to create a planar-like model that can balance on one foot. The parameter ω_1 affects the perpendicular distance in the x direction of a link from the pelvis (i.e., if the perpendicular distance of link i from the pelvis was δx_i , then the model would contain the product $\omega_1 \delta x_i$), ω_2 affects the perpendicular distance in the x direction of a link’s center of mass from the pelvis, and ω_3 affects the perpendicular distance in the y direction of the center of mass from the pelvis for the back and neck links. The value of ω_3 has to be fixed at zero in order to achieve period-one walking gaits. When all three parameters are zero, they eliminate the non-zero moments about the joints due to the gravity vector making the configuration depicted in Figure 2.9(b) an equilibrium gait for the model. A value of one for each parameter gives the original biped model.

In total, the biped has a 17-dimensional state-time-control space \mathcal{S} . With our parameter space \mathcal{S} defined, we can now generate gaits for Atlas using the same process as we did with the compass gait. Our particular Atlas model has a singular EG at $\tau = 0.655$ s, which we found using Algorithm 2. We then performed a NCM using the map M_0 starting

at the singular EG at $\tau = 0.655$ s. A gait from this continuation is shown in Figure 2.4(g). The biped is shown taking two steps.

As with the compass-gait walker, we could then use this branch of gaits to grow the set of gaits available to Atlas by allowing the parameters in μ to vary or by adding more control parameters. The GHM could then be used to define a 1D map that could be used with Algorithm 1 to search for desired gaits on the higher-dimensional submanifold.

2.5.4. Incorporating Inequality Constraints

In this example, we use the University of Michigan’s MARLO biped robot [31, 62] (Figure 2.9(a)) to demonstrate how to incorporate inequality constraints into a continuation. The biped MARLO is part of a line of ATRIAS bipeds developed at Oregon State University [37]. The hybrid dynamics of the model is detailed in [62]. We do not model the series elastic actuators, but do take into account the mass of the actuators. The physical parameters for our model are taken from the source code in [30], which is used in [31].

The biped MARLO has 16 degrees-of-freedom (DOFs) when no constraints are applied. The biped walks in the y - z plane (its sagittal plane) with gravity pointing in the negative z direction. Referring to Figure 2.9(a), the joints of the biped are a 6-DOF floating base (where q_1 - q_3 are the roll, pitch, and yaw angles, respectively), two hip joints for out-of-plane leg rotation (q_4 - q_5), and eight joints for the two four-bar mechanisms serving as legs for the biped (q_6 - q_{13}). When constraints are applied, MARLO has seven PHCs ($n_p = 7$). Three of the constraints cause the biped to pivot about its stance foot and the other four constraints are the four-bar linkage constraints on each leg:

$$\begin{aligned} q_6 + q_{10} - q_7 &= 0 & q_7 + q_{11} - q_6 &= 0 \\ q_8 + q_{12} - q_9 &= 0 & q_9 + q_{14} - q_8 &= 0. \end{aligned}$$

Given these constraints, we can describe a pre-impact state $x_0 \in \mathcal{X}$ of the biped using 18 numbers, the nine joint angles q_1 - q_9 and their respective velocities ($n = 9$).

The biped has six actuators located at its hip, shin, and thigh joints q_4 - q_9 ($n_u = 6$) and is subject to six virtual holonomic constraints ($n_v = 6$). When the left leg is the

stance leg the constraints are:

$$(2.15) \quad \begin{aligned} q_4 - b_4^3(s, a) = 0 & \quad q_5 - b_5^3(s, a) = 0 & \quad q_6 - b_6^3(s, a) = 0 \\ q_{10} - b_{10}^3(s, a) = 0 & \quad q_8 - b_8^4(s, a) = 0 & \quad q_{12} - b_{12}^4(s, a) = 0, \end{aligned}$$

and similarly for when the right leg is in stance.

During a step, the VHCs force the hip, stance thigh, and lower leg to track third-order Bézier polynomials and the swing thigh and lower leg to track fourth-order Bézier polynomials. The two fourth-order polynomials $b_8^4(s, a)$ and $b_{12}^4(s, a)$ each have a free coefficient that is not determined by the periodicity boundary constraints. The two free coefficients, say $\alpha_1, \alpha_2 \in \mathbb{R}$, are made part of the parameter control subspace in \mathcal{S} .

Overall, there are six control parameters $\mu = [\omega, s_1, s_2, s_3, \alpha_1, \alpha_2]^T \in \mathcal{M} \subseteq \mathbb{R}^k$ ($k = 6$). The dimensionless parameter $\omega \in \mathbb{R}$ continuously deforms the physical parameters of the biped from a planar model into a 3D model by controlling the hip width and the position of the center of mass of each link on the biped (in other words, if the hip width is defined by the physical parameter ℓ_{hip} , then the model would have its hip width defined as the product $\omega \ell_{\text{hip}}$). Figure 2.10 depicts how ω affects the biped's hip width; it does not show the effects on the center of mass of each link. At $\omega = 0$, the biped has zero hip width and all of the center of masses are projected onto their respective links. When we have $\omega = 1$, the original values for the biped's hip width and link center of masses are restored.

Finally, the design and control parameter vector μ has three slack variables $s_1, s_2, s_3 \in \mathbb{R}$ with lower bounds $s_1, s_2, s_3 \geq 0$; there are no upper bounds on the variables. These constraints can be treated as box constraints [56]. We use the slack variables s_1 and s_2 so that we only search for gaits where the knee joints q_{10} and q_{12} are nonnegative pre-impact. We find this is sufficient to avoid knee hyperextension as the biped takes its step ($q_{10}(t), q_{12}(t) \leq 0$ for all t). The third slack variable s_3 is used to make sure the biped walks from left to right by imposing a forward velocity constraint on the biped's floating base $q_y \in \mathbb{R}$ coordinate.

For box constraints imposed on the values of a vector in the state-time-control space $c \in \mathcal{S}$, we use the projected Newton's method [5] to enforce the constraints during the

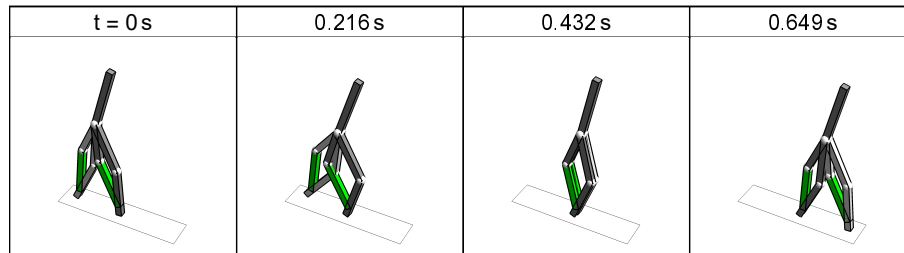
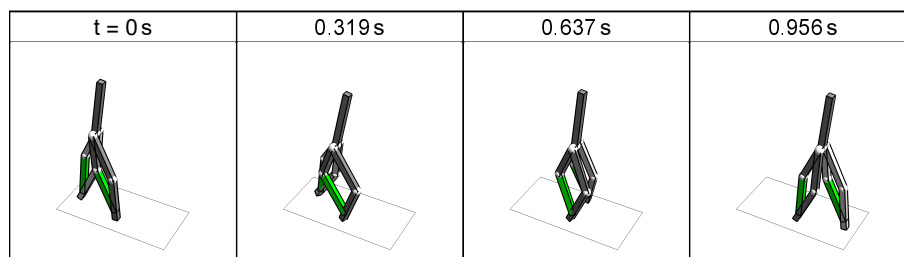
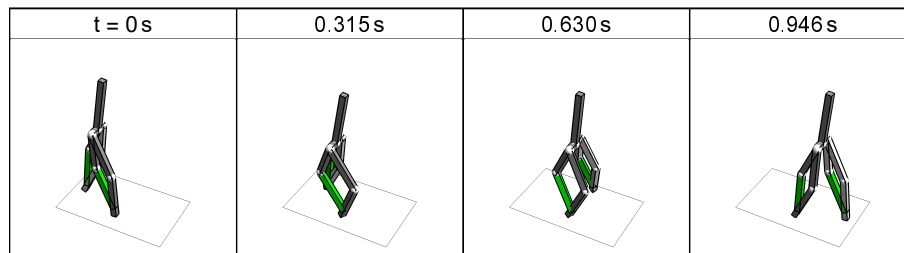
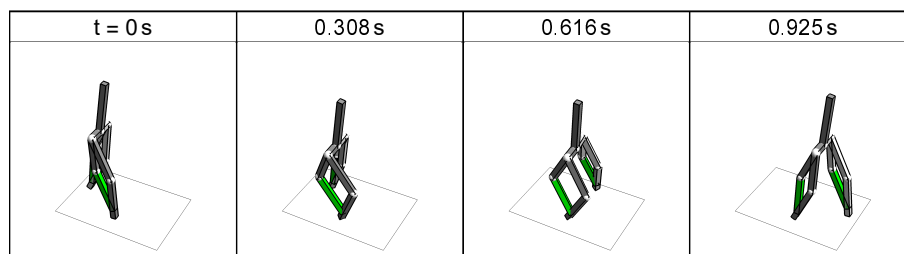
(a) $\omega = 0.11$ (b) $\omega = 0.37$ (c) $\omega = 0.65$ (d) $\omega = 1$

Figure 2.10. The effect of the parameter ω on the hip width of MARLO. The parameter also affects the position of the center of mass of each link (not shown).

call to Newton’s method in lines 6–7 of Algorithm 1. Algorithm 1 would be modified to accept lower and upper bounds on the values of the vector $c \in \mathcal{S}$.

Imposing box constraints on c may not be enough to, for example, avoid the biped’s swing foot from penetrating the walking surface. Let $p(t) = p(\varphi_\mu^t(x_0)) \in \mathbb{R}^3$ represent the location of the swing foot in space, and $\text{dist}(p(t)) \in \mathbb{R}$ be a distance function that is positive when the swing foot is above the surface, zero when the swing foot is on the surface, and negative when the swing foot is below the surface. To avoid foot penetration we require $\text{dist}(p(t)) \geq 0$ for all $t \in \mathbb{R}$. This is equivalent to finding the zeros of $\int_0^\tau [\text{dist}(p(t))]^- dt$, where $[x]^-$ returns x if $x \leq 0$ and zero otherwise.

Given the biped model and its PHCs and VHCs, the resulting state-time-control space \mathcal{S} is 25 dimensional (18 state variables, 6 design and control parameters, and 1 switching time). The biped’s periodicity map P is

$$P(c) = \begin{bmatrix} Q_1 \\ \dot{Q}_1 \end{bmatrix}, \quad Q_1 = \begin{bmatrix} q_1(\tau^-) - q_1(0^-) \\ q_2(\tau^-) - q_2(0^-) \\ q_3(\tau^-) - q_3(0^-) \end{bmatrix},$$

which states that the roll, pitch, and yaw angles of the floating base have to be periodic. These are the only angles that are unactuated; all other angles are subject to VHCs for which we can by design satisfy the periodicity condition of the (virtually) constrained joints [78].

The manifolds in the gait space \mathcal{G} are 19 dimensional (25 state-time-control variables minus 6 periodicity constraints). We cannot apply Algorithm 2 because $\frac{\partial P}{\partial x_0}(c) \in \mathbb{R}^{6 \times 18}$ is not a square matrix. We demonstrate the utility of searching for locomoting gaits on a high-dimensional manifold using the Global Homotopy Map (GHM) as input to the pseudo-arclength NCM. As an additional benefit, we can start from any EG with an arbitrarily chosen switching time τ as long as the equilibrium gait isn’t a minimizer with respect to the cost function of Equation 2.12. For use in the continuation, we define two GHM maps similar to Equation 2.11. The desired gaits we search for using these maps reflect equality and inequality constraints encountered in the literature [6, 36, 58, 62, 78] (e.g., gaits that walk on flat ground).

The first map we use with Algorithm 1, $M_a^1 : \mathcal{S} \rightarrow \mathbb{R}^{18}$, generates a desired gait starting from an EG of the planarized version of biped model ($\omega = 0$), where $M_a^1(c) = [P(c)^T, \Phi_1(c)^T, H_1(c)^T - H_1(a, p(c, a))^T]^T$ such that the map P is the biped's periodicity map, $p(c, a) \in \mathbb{R}$ is the homotopy parameter (Equation 2.9), $\Phi_1 : \mathcal{S} \rightarrow \mathbb{R}^7$

$$\Phi_1(c) = \begin{bmatrix} q_6(0^-) - q_7(0^-) - s_1 \\ q_8(0^-) - q_9(0^-) - s_2 \\ \dot{q}_y(0^-) - s_3 \\ q_1(0^-) \\ q_2(0^-) \\ q_4(0^-) \\ q_5(0^-) \end{bmatrix}$$

is a map of three inequality constraints and four equality constraints that defines the properties that each gait in $\mathcal{G}_{\text{mapped}}$ have in common; the first two constraints ensure the left and right knee joints bend inward in an anthropomorphic manner, the third constraint ensures the biped travels from left to right with a positive forward velocity, and the last four constraints ensure the out-of-plane angles (including those of the floating base) start and end at zero degrees, and $H_1 : \mathcal{S} \rightarrow \mathbb{R}^5$

$$H_1(c) = \begin{bmatrix} s_1 - s_{1,\text{des}} \\ s_2 - s_{2,\text{des}} \\ \sigma(c) - \sigma_{\text{des}} \\ q_y(\tau^-) - q_y(0^-) - q_{y,\text{des}} \\ \int_0^\tau [\text{dist}(p(t))]^- dt \end{bmatrix}$$

is used to guide the continuation on the submanifold defined by Φ_1 and containing the initial EG to find a gait with a desired knee bend ($s_{1,\text{des}} = s_{2,\text{des}} = 20^\circ$), desired walking surface ($\sigma_{\text{des}} = 0 \in \mathbb{R}^2$, i.e., a flat ground), desired step length ($q_{y,\text{des}} = 0.5$ m), and desired minimum height above the ground for the swing foot during a step ($\text{dist}(p(t)) > 0$). Figure 2.10(a) is the resulting gait starting from an EG of $a = (0, 0.5) \in E$, where a

corresponds to a planar biped model in its equilibrium stance and defines the homotopy parameter $p(c, a)$ for M_a^1 .

Starting from the gait shown in Figure 2.10(a), we use our second GHM map M_a^2 to continuously deform our gait found with the previous map into a gait with the biped's original physical parameters (e.g., we want to find a gait in \mathcal{G} with $\omega = 1$), where $M_a^2(c) = [P(c)^T, \Phi_2(c)^T, H_2(c)^T - H_2(a, p(c, a))^T]^T$ and

$$\Phi_2(c) = \begin{bmatrix} \Phi_1(c) \\ \sigma(c) - \sigma_{\text{des}} \\ \int_0^T [\text{dist}(p(t))]^- dt \end{bmatrix}, \quad H_2(c) = \begin{bmatrix} s_1 - s_{1,\text{des}} \\ s_2 - s_{2,\text{des}} \\ q_y(\tau^-) - q_y(0^-) - q_{y,\text{des}} \\ \omega - 1 \end{bmatrix},$$

where $\Phi_2(c) \in \mathbb{R}^9$ is a set of constraints and $H_2(c) \in \mathbb{R}^4$ guides the NCM to find a gait with the biped's original hip width and positions of center of mass of each link. Figure 2.10 shows the deformation of gaits in $\mathcal{G}_{\text{mapped}}$ starting from the desired gait found using M_a^1 with $\omega = 0.11$ to the original 3D model ($\omega = 1$).

2.6. Conclusion

We present a robust method for generating a manifold of walking gaits using numerical continuation methods based on the connected component of an equilibrium fixed point of a multi-degree-of-freedom bipedal robot (that of standing still). Our approach differs from other gait generation algorithms in that we transform the problem of gait generation to generating a connected surface (or level set) of periodic walking gaits. The major advantage is that we give an initial stance for finding nearby walking gaits for bipeds subject to physical and virtual holonomic constraints regardless of the degrees of freedom in the model. We prove that the dimension of the search space for an initial gait is one dimensional and is only dependent on the period of the gait. We preserve the ‘‘natural’’ dynamics of the hybrid system producing passive dynamic walking gaits. We can also incorporate control and design parameters, which can generate a diverse set of periodic walking motions (e.g., actuated and 3D gaits) using virtual holonomic constraints. As examples, we show how our algorithm can generate numerous gaits for the compass-gait, Atlas, MARLO bipeds.

For future work, we plan on having a more in-depth analysis of our approach with respect to optimization methods. While the main goal of this paper is to introduce the main concepts and algorithms of our framework, we want to compare the performance of our approach to state-of-the-art optimization packages cited in the literature in future work. In particular, we want to compare our method to DIRCOL [58] and FROST [36] as these two packages generate gaits for limit cycle walkers given their respective frameworks.

A few benefits of the algorithms presented in this paper, unlike other gait generation routines, are that we do not rely on special software such as SNOPT or IPOPT, a particular integration scheme to solve for the hybrid dynamics (as is the case with direct collocation methods), and can reliably generate gaits using only first-order derivative information of the hybrid dynamics (which can be a useful feature when computing the Hessian is prohibitively expensive, as can be the case for high-degree-of-freedom humanoid robots). A free implementation of our framework can be found online [66]. It can be used with any biped model subject to physical and virtual holonomic constraints that can be represented as a kinematic tree of rigid bodies [20].

And while we claim that our algorithms are simpler to implement, in this paper we demonstrate that given a parameterized space of trajectories \mathcal{S} , we, to the best of our knowledge, are the first to characterize the set of gaits (periodic motions that satisfy a biped’s hybrid dynamics) in the parameter space. Our analysis has led to the premise that certain equilibria of a biped can be used as motion generators, which can be used by any gait generation algorithm to generate a path-connected set of walking gaits through a continuous deformation of the parameters that define the space \mathcal{S} .

2.7. Appendix A: Biped as Constrained Mechanical Systems

In Section 2.3, we defined the hybrid dynamics Σ as the tuple $\Sigma = (\mathcal{X}, f, \Delta, \phi)$, where $f : \mathcal{X} \times \mathbb{R}^{n_u} \rightarrow T\mathcal{X}$ is a vector field on \mathcal{X} , $\Delta : \mathcal{X} \rightarrow \mathcal{X}$ is a jump map mapping pre- to post-impact states, and $\phi : \mathbb{R} \times \mathcal{X} \rightarrow \mathbb{R}$ is a switching function which determines when an impact occurs. The goal of this section is to derive f and Δ in terms of the Euler-Lagrange equations for constrained mechanical systems [1, 17, 45].

2.7.1. The Vector Field f

We model the continuous dynamics of an n -degree-of-freedom biped as a constrained mechanical system subject to n_p physical and n_v virtual holonomic constraints ($n_p, n_v \geq 0$). For a biped's continuous dynamic regime, we assume that the state of the biped $x = (q, \dot{q}) \in \mathcal{X}$ is known and that the biped is subject to a set of physical and virtual holonomic constraints $h_p(q) = 0 \in \mathbb{R}^{n_p}$ and $h_v(q) = 0 \in \mathbb{R}^{n_v}$, respectively. The state x , accelerations $\ddot{q} \in \mathbb{R}^n$, constraint forces $\lambda \in \mathbb{R}^{n_p}$, and control inputs $u \in \mathbb{R}^{n_u}$ ($n_u \geq n_v$) of the continuous dynamics satisfy

$$(2.16) \quad \begin{aligned} M(q)\ddot{q} + b(q, \dot{q}) &= J_p(q)^T \lambda + B_v(q)u, \\ \dot{J}_p(q)\dot{q} + J_p(q)\ddot{q} &= 0, \quad \dot{J}_v(q)\dot{q} + J_v(q)\ddot{q} = -v(q, \dot{q}), \end{aligned}$$

where $M(q) \in \mathbb{R}^{n \times n}$ is the mass matrix, $b(q, \dot{q}) \in \mathbb{R}^n$ is a vector of the centrifugal, Coriolis, and gravitational forces, $B_v(q) \in \mathbb{R}^{n \times n_u}$ is a transmission matrix, $J_p(q) = \frac{\partial h_p}{\partial q}(q) \in \mathbb{R}^{n_p \times n}$ and $J_v(q) = \frac{\partial h_v}{\partial q}(q) \in \mathbb{R}^{n_v \times n}$ are the constraint Jacobian for the physical and virtual constraints, respectively, and $v(q, \dot{q}) \in \mathbb{R}^{n_v}$ is a linear feedback controller for stabilizing the virtual constraints. An example PD control law for $v(q, \dot{q})$ used in [36, 78] is

$$v(q, \dot{q}) = \frac{1}{\epsilon} K_D J_v(q) \dot{q} + \frac{1}{\epsilon^2} K_P h_v(q),$$

where $h_v(q) \in \mathbb{R}^{n_v}$ are VHCs, $K_P, K_D \in \mathbb{R}^{n_v \times n_v}$ are positive definite matrices and $\epsilon \in \mathbb{R}$ is a positive scalar tuning parameter which can speed up convergence to the origin, $h_v(q) = J_v(q)\dot{q} = 0$.

Given Equation 2.16, the vector field f is then $f(x, u) = (\dot{q}, \ddot{q})$, where \ddot{q} is the solution to

$$\begin{bmatrix} M(q) & -J_p(q)^T & -B(q) \\ J_p(q) & 0 & 0 \\ J_v(q) & 0 & 0 \end{bmatrix} \begin{bmatrix} \ddot{q} \\ \lambda \\ u \end{bmatrix} = - \begin{bmatrix} b(q, \dot{q}) \\ 0 \\ v(q, \dot{q}) + J_v(q)\dot{q} \end{bmatrix},$$

which is a linear system of equations with $n + n_p + n_v$ equations in $n + n_p + n_u$ unknowns. A solution exists with a generalized right inverse (we use the Moore-Penrose Inverse) as long as the matrix on the left-hand side has maximal rank $n + n_p + n_v$.

Remark 7. The differential form of the virtual constraints $\dot{J}_v(q)\dot{q} + J_v(q)\ddot{q} = -v(q, \dot{q})$ can model virtual holonomic *and* nonholonomic constraints. Similarly for the differential form of the physical constraints.

Remark 8. A linear stabilizing feedback controller $v_p(q, \dot{q})$ can also be defined for the n_p physical constraints such that $\dot{J}_p(q)\dot{q} + J_p(q)\ddot{q} = -v_p(q, \dot{q})$ in order to reduce constraint violations during simulations due to numerical rounding errors. For example, it would be straightforward to implement Baumgarte’s constraint stabilization technique [4] using the form of the feedback law for $v(q, \dot{q})$. Other options also exist [16].

Remark 9. The solution to $u(t)$ of Equation 2.16 is equivalent to the solution of a stabilizing feedback linearizing control law used to enforce VHCs in the Hybrid Zero Dynamics framework [78] with $v(q, \dot{q})$ as the linear control law.

2.7.2. The Jump Map Δ

We model collisions as a set of impulsive algebraic equations, namely the impulse-momentum equations in generalized coordinates along with a set of plastic impact equations needed to uniquely solve for the impulse and post-impact velocities. During a collision at time $t \in \mathbb{R}$, we assume the pre-impact state of the biped $x(t^-) = (q, \dot{q}) \in \mathcal{X}$ is known. The pre-impact state $x(t^-)$, post-impact state $x(t^+) = (q^+, \dot{q}^+) \in \mathcal{X}$, and impulses $\iota \in \mathbb{R}^{n_\iota}$ of the impulse equations satisfy

$$\begin{aligned} q^+ &= q \\ M(q)(\dot{q}^+ - \dot{q}) &= J_\iota(q)^T \iota \\ J_\iota(q)\dot{q}^+ &= 0, \end{aligned}$$

where $J_\iota \in \mathbb{R}^{n_\iota \times n}$ is the constraint Jacobian that maps the post-impact velocities to contact velocities.

The jump map Δ is then $\Delta(x) = (q, \dot{q}^+)$, where \dot{q}^+ is the solution to

$$\begin{bmatrix} M(q) & -J_\iota(q)^T \\ J_\iota(q) & 0 \end{bmatrix} \begin{bmatrix} \dot{q}^+ \\ \iota \end{bmatrix} = \begin{bmatrix} M(q)\dot{q} \\ 0 \end{bmatrix},$$

which is a linear system of equations with $n + n_l$ equations in $n + n_l$ unknowns. A unique solution exists as long as J_l has maximal rank n_l .

For most bipeds, $J_l = J_p$. In general, any Jacobian J_l is fine as long as the set of jump map constraints are more restrictive than the PHC constraints, i.e., $\{x \in \mathcal{X} : J_l(q)\dot{q}\} \subseteq \{x \in \mathcal{X} : J_p(q)\dot{q}\}$.

2.8. Appendix B: Extended Proofs of the Equilibrium Branches of M_0

Proposition 5. *Given:*

- (1) A biped's hybrid dynamics $\Sigma = (\mathcal{X}, f, \Delta, \phi)$,
- (2) An equilibrium point $x_{eq} \in \mathcal{X}$ of f ,
- (3) A switching time $\tau_0 \in \mathbb{R}$, and
- (4) A vector of input parameters $\mu_0 \in \mathbb{R}^k$

such that $M_0(c_0) = 0$, where $c_0 = (x_{eq}, \tau_0, \mu_0) \in E_0$. If c_0 is a regular point of M_0 , then there exists a unique curve $c : (-\delta, \delta) \rightarrow E_0$ contained in E_0 that passes through c_0 at $c(0) = c_0$ for some $\delta > 0 \in \mathbb{R} \cup \{\infty\}$.

PROOF. It follows from the implicit function theorem (IFT, [74]) that there exists a unique curve c passing through c_0 . What remains to be shown is that the points on the curve are all in E_0 . From the IFT, we conclude that in an open neighborhood $A \subseteq \mathbb{R}$ containing τ_0 and an open neighborhood $B \subseteq \mathbb{R}^{2n+k}$ containing the pair (x_{eq}, μ_0) that for each $\tau(s) \in A$ there exists a unique $g(\tau(s)) \in B$ such that $g(\tau) = (x_0(\tau), \mu_0(\tau))$, $c(s) = (x_0(\tau(s)), \tau(s), \mu_0(\tau(s)))$ and $M_0(c(s)) = 0$ for some parameterization of $s \in (-\delta, \delta)$.

We determine g from the Jacobian J_0 of M_0

$$(2.17) \quad J_0(c) = \begin{bmatrix} \frac{\partial P}{\partial c}(c) \\ \frac{\partial \Phi_0}{\partial c}(c) \end{bmatrix} = \begin{bmatrix} \frac{\partial P}{\partial x_0}(c) & \frac{\partial P}{\partial \tau}(c) & \frac{\partial P}{\partial \mu}(c) \\ 0 & 0 & I_k \end{bmatrix}.$$

Given that x_{eq} is an equilibrium point, we have at $J(c_0)$

$$\frac{\partial P}{\partial \tau}(p(s_0)) = f(x_{eq}, u(\tau(s_0))) \frac{\partial \tau}{\partial c}(p(s_0)) = 0.$$

Additionally, because c_0 is a regular point of M_0 , the submatrix

$$\bar{J} = \begin{bmatrix} \frac{\partial P}{\partial x_0}(c_0) & \frac{\partial P}{\partial \mu}(c_0) \\ 0 & I_k \end{bmatrix}$$

must be full rank, $\det(\bar{J}) \neq 0$, otherwise J_0 cannot have maximal rank and c_0 would be a singular point, which it is not. From these two facts, the IFT states that g must be the solution to the IVP

$$g(\tau_0) = (x_{\text{eq}}, \mu_0), \quad \frac{\partial g}{\partial \tau}(\tau) = - \begin{bmatrix} \frac{\partial P}{\partial x_0}(p(s_0)) & \frac{\partial P}{\partial \mu}(p(s_0)) \\ 0 & I_k \end{bmatrix}^{-1} \begin{bmatrix} \frac{\partial P}{\partial \tau}(p(s_0)) \\ 0 \end{bmatrix} = 0,$$

which gives $g(\tau(s)) = (x_{\text{eq}}, \mu_0)$ for all $\tau(s) \in \mathbb{R}$.

To finish describing the curve c , we now determine an expression for $\tau = \tau(s)$ valid for $s \in (-\delta, \delta)$. Given an arclength parameterization of the curve c , the tangent to the curve c at c_0 is $\frac{dc}{ds}(0)$ and it is the only vector in the tangent space $T_{c_0}M_0$. As the tangent space is equal to the null space of $J_0(c_0)$, we have

$$(2.18) \quad \text{Null}(J_0(c_0)) = \text{Null} \left(\begin{bmatrix} \frac{\partial P}{\partial x_0}(c) & 0 & \frac{\partial P}{\partial \mu}(c) \\ 0 & 0 & I_k \end{bmatrix} \right) = \{ [0_{2n}, 1, 0_k]^T \},$$

where 0_k is a vector with k zeros and similarly for 0_{2n} . Hence, $\frac{d\tau}{ds}(s) = 1$ and for $\tau(0) = \tau_0$, $\tau(s) = \tau_0 + s$.

Therefore, $c(s) = (x_{\text{eq}}, \tau_0 + s, \mu_0)$ for $s \in (-\delta, \delta)$, which are all in E_0 and by the IFT are the only points in a neighborhood containing c_0 that are in \mathcal{G}_0 . \square

Proposition 6. *Assume there exists a path $p : [0, 1] \rightarrow \mathcal{G}_0$ such that $p(0) \in E_0$, and $p(1) \in \mathcal{G}_0 - E_0$. If $p(0)$ is a regular point of M_0 , then*

- (1) *The path p contains at least one singular equilibrium point $p(s) \in E_0$, and*
- (2) *For each singular equilibrium point $p(s) \in E_0$ for $s \in (0, 1)$ the $\det(\frac{\partial P}{\partial x_0}(p(s))) = 0$.*

PROOF. We prove the first claim by showing that the path p can never have points in $\mathcal{G}_0 - E_0$ if EGs on the path are regular points of M_0 . The second claim is proven through a direct computation.

Assume there exists a path p with $p(0) \in E_0$ and $p(1) \in \mathcal{G}_0 - E_0$ such that all EGs in p are regular points of M_0 . Then by Proposition 1 because $c_0 \in E_0$ is a regular point of M_0 , then any path $p : [0, 1] \rightarrow \mathcal{G}_0$ starting at c_0 must coincide locally with the unique curve $c : (-\delta, \delta) \rightarrow E_0$. As the functions p and c coincide but have different domains, assume that $s \in [0, s_\delta)$ continuously maps to $\alpha(s) \in (-\delta, \delta)$ such that for $s = 0$ we have $\alpha(0) = 0$.

Consider p at $s = s_\delta$, because p is continuous $p(s_\delta)$ must be equal to the left-sided limit of p at s_δ that is $p(s_\delta) = \lim_{s \nearrow s_\delta} (x_{\text{eq}}, \tau_0 + \alpha(s), \mu_0) = (x_{\text{eq}}, \tau_0 + \alpha(s_\delta), \mu_0)$. Therefore, $p(s_\delta)$ is an EG in E_0 , but by assumption it is also a regular point of M_0 , so we can apply Proposition 1 and conclude that the interval over which p and c have to coincide extends beyond $s \in (0, s_\delta)$ for the path p .

In other words, the unique curve c passing through $c(0)$ can be extended past the open interval $(-\delta, \delta)$. In fact, there is no finite value of δ that can contain the entire interval of c as its limit points $c(\delta) = p(s_\delta) \in E_0$ are regular points of M_0 . The curve can always be extended and as the curve c is unique, the path p has no choice but to follow it. The path p however is finite with its points determined by c over its finite interval, but, for $s \in [0, 1]$, $p(s) \in E_0$. This contradicts our main assumption that $p(1) \in \mathcal{G}_0 - E_0$ given that all EGs are regular points of M_0 .

Therefore, there must exist at least one singular EG on the path p . In order for a point $p(s) \in E_0$ in the path p to be singular, we need the submatrix \bar{J} of the Jacobian J_0 evaluated at $p(s)$

$$\bar{J}(p(s)) = \begin{bmatrix} \frac{\partial P}{\partial x_0}(p(s)) & \frac{\partial P}{\partial \mu}(p(s)) \\ 0 & I_k \end{bmatrix}$$

to not be invertible so that the IFT (and Proposition 1) does not apply. For any $p(s)$ that is a singular EG of M_0 , this can only happen if

$$\det \left(\begin{bmatrix} \frac{\partial P}{\partial x_0}(c_s) & \frac{\partial P}{\partial \mu}(c_s) \\ 0 & I_k \end{bmatrix} \right) = \det \left(\frac{\partial P}{\partial x_0}(c_s) \right) = 0.$$

□

CHAPTER 3

The Passive Dynamics of Walking and Brachiating Robots: Results on the Topology and Stability of Passive Gaits

This chapter is published in [65]. It explores the multi-locomotion capabilities of a two-link biped that can use its limbs as feet to walk or as hands to swing around in its environment. Humanoids and ape-inspired robots are example bipeds that can use their arms and legs to locomote in their surroundings [9, 48]. For a generalized two-link robot that can walk and brachiate, this paper explores the types of gaits available to the robot starting from gaits that perform zero work (i.e., gaits that impact at zero velocity). The paper serves as an example of the type of analysis and conclusions that can be drawn by studying the connected components of a biped robot that can use its limbs as feet to walk or as hands to swing around in its environment. The contributions of this chapter to the thesis are

- (1) A means for describing an equivalency class of gaits in the state-time-control space of the biped model. Two gaits are equivalent if there exists a path from one to the other. Either gait can serve as a motion generator for the other.
- (2) A proof that gaits in the two-link robot's parameter space can be partitioned into two classes of gaits: one that resembles walking (where the link's cross each other at some point in its trajectory) and another that resembles underhand brachiation (where the links do not cross).
- (3) The effects on the open-loop stability of a family of gaits subject to state- and time-based switching. We show differences in stability, bifurcations, and routes to chaos for state- vs. time-based switched system.

3.1. Abstract

Simple walking models, like the compass-gait model, have yielded useful insight into the basic mechanics of walking. A similar model serves as a template for brachiation. With the ability of a two-link robot to walk and swing, we explore the multi-locomotion capability of a generalized two-link model with potential footholds at any location. We focus on the connected components of passive gaits in a five-dimensional state-time space. Our main results are: (1) a walking gait and a brachiating gait cannot be in the same connected component and (2) the stability of a gait depends on whether impacts are state-based (e.g., footfall in a biped walker) or time-based (e.g., time between clamping brachiator hands to a wall). For the same connected component of gaits, the different impact types result in different bifurcations.

3.2. Introduction

We study the passive hybrid dynamics of planar, single-joint, two-link walking and brachiating robot models. These simplified models of walking and brachiating have been studied extensively in the past [22, 25, 26, 67]. These locomotors are modeled as a hybrid system, where two continuous swing motions are separated by an impact with a surface causing a discontinuous jump in velocity.

We generalize the two-link walking models [22, 26] and brachiator models [25, 54] to a single model that can both walk and brachiate. This allows us to study robots like our wall-climbing Gibbot robot [67], which can achieve a “foothold” anywhere on a vertical plane. Since the “feet” of the generalized model can achieve a foothold at any location on a vertical plane, we can study two impact strategies: switching the stance foot when (1) it “collides” with a fixed virtual slope (state-based impacts) or (2) a set period of time has elapsed (time-based impacts). Figure 3.1 shows a simple two-link model walking and brachiating on the same downhill slope.

In the past, simple two-link models have successfully guided the design of several walking and brachiating robots [8, 54, 55, 77]. Yet, with the exception of work by Fukuda et al. [21], walking and brachiating robots are treated separately because of their distinct

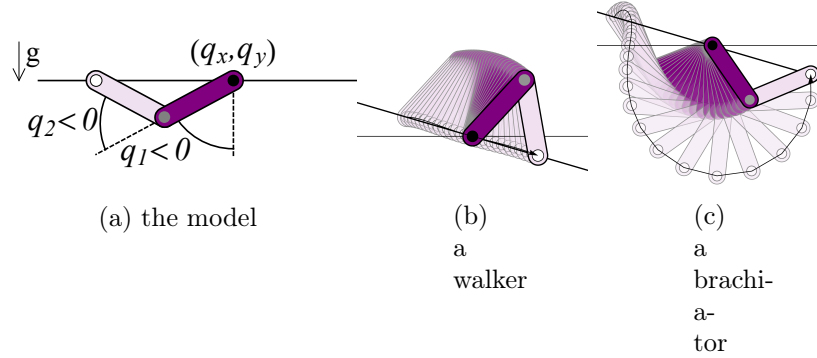


Figure 3.1. An example of (a) the two-link model (b) walking and (c) brachiating on the same downhill slope. The swing leg is the lightly shaded link.

environments. Given our generalized model, could walking and brachiating gaits actually be considered examples of the same type of gait? Furthermore, the same gait can be achieved by either state-based or time-based impact. But is there a difference in stability depending on the type of impact?

We address these two questions by studying the connected components and stability of gaits in our generalized model. We define a gait as a period-one fixed point of the hybrid dynamics in a five-dimensional state-time space. For a period-one fixed point, the state corresponds to the robot's post-impact state at the beginning of a new swing and time corresponds to the period of time between impacts. Gaits in the same connected component have a path connecting them.

Definition 5. A *path* between two gaits a and b is a continuous function f from the unit interval $[0, 1]$ to the set of gaits in \mathbb{R}^5 such that $f(0) = a$ and $f(1) = b$.

If a path exists between two gaits, then it is possible to continuously deform one gait into the other. We give an example in Section 3.4.

Similar to the terminology used in the walking community, we refer to the link that is in contact with the surface as the stance leg and the other link as the swing leg. After an impact the roles of the two links switch. For motions of the swing leg relative to the stance leg where the net displacement does not exceed one revolution during a step,

the net displacement can only have two possible values. These values map the swing leg trajectory to a net motion where the links cross once or not at all. We define walking and brachiating gaits based on this notion of links crossing.

Definition 6. The links *cross* when the net angular displacement of the swing leg relative to the stance leg does not equal the difference between the final and initial angles of the swing leg relative to the stance leg. For a *walking* gait, the links cross. For a *brachiating* gait, the links do not cross.

We return to this definition in Section 3.4. Our contributions are

- (1) **Walking and brachiating fixed points are not in the same connected component of gaits.** We show that walking and brachiating gaits are two disjoint sets. We explore a connected component in each set through numerical simulation and show that both gaits can passively locomote above or below a fixed slope. For example, we show that it is possible to continuously deform a walking gait that walks on ground to a gait that passively “walks” on an inclined ceiling.
- (2) **The impact strategy affects the stability of a gait.** We find that state-based switching leads to more stable gaits than time-based switching. When gaits become unstable, state-based switching leads to period-doubling bifurcations (stable period- $2n$ gaits, $n \geq 1$), and time-based switching leads to Neimark-Sacker bifurcations (n -periodic or quasiperiodic gaits, $n > 1$).

We define the hybrid dynamics of the system in Section 3.3. In Sections 3.4 and Section 3.5 we show (1) and (2), respectively. We conclude in Section 3.6.

3.3. The Hybrid Dynamics

The physical parameters of each link of the robot are identical to each other, which allows us to define a gait in half a swing of the robot. The configuration vector (Figure 3.1(a)) of the robot is $q' = [q_x, q_y, q_1, q_2]^T$, where (q_x, q_y) are the x - y coordinates of the stance leg in a world frame, q_1 is the angle of the stance leg from the vertical, and q_2 is the angle of the swing leg relative to the stance leg. The pivot point (q_x, q_y) remains

fixed throughout the swing motion. For convenience, during the swing we use a reduced configuration vector $q = [q_1, q_2]^T$ with state vector $x = [q^T, \dot{q}^T]^T$. We define the flow of the continuous dynamics of the double pendulum as

$$x(x_0, t) = x_0 + \int_0^t F(x(s)) ds,$$

where x_0 is the initial state of the robot at time $s = 0$, t is the impact time, and $F(x(s)) = [\dot{q}(s)^T, \ddot{q}(s)^T]^T$.

When the robot impacts, it undergoes an instantaneous, plastic impact. The configuration of the robot does not change, but its velocity does. The impact map H relates the pre-impact state to the post-impact state of the robot at the time of impact and is defined as

$$H(x) = \begin{bmatrix} A & 0 \\ 0 & P(q) \end{bmatrix} x + \begin{bmatrix} b^T & 0 & 0 \end{bmatrix}^T,$$

where $A = \begin{bmatrix} 1 & \\ & -1 \end{bmatrix} \in \mathbb{R}^{2 \times 2}$ and $b = \begin{bmatrix} \pi \\ 0 \end{bmatrix} \in \mathbb{R}^2$ flip the coordinate system, and $P(q) \in \mathbb{R}^{2 \times 2}$ relates the pre-impact velocity \dot{q}^- to the post-impact velocity \dot{q}^+ such that $\dot{q}^+ = P(q^-)\dot{q}^-$. A detailed derivation of the equations and parameters used for our two-link model can be found in a previous paper [67].

In sum, the hybrid system is written as a discrete map $G: \mathbb{R}^4 \times \mathbb{R} \rightarrow \mathbb{R}^4$

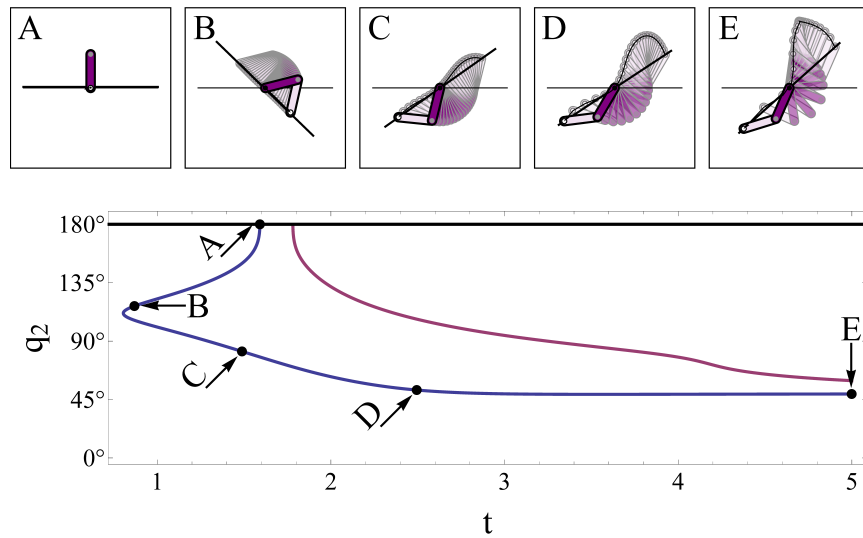
$$x_1 = H(x(x_0, t)) = G(x_0, t),$$

where x_0 is the initial state, $x(x_0, t)$ is the pre-impact state, and x_1 is the final state after the impact at time t . A ‘‘gait’’ is a period-one fixed point (x_0^*, t^*) satisfying $x_0^* = G(x_0^*, t^*)$. The fixed point is stable if the maximum eigenvalue of $\frac{\partial G}{\partial x_0}(x_0^*, t^*)$ is inside the unit circle.

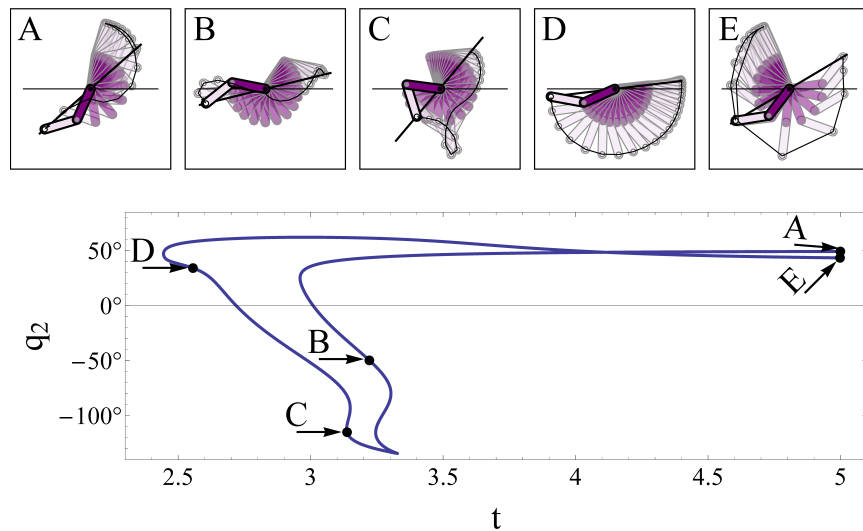
3.4. Connected Components in the State-Time Space

In our search for gaits, we allow the state and impact time to vary. In this five-dimensional state-time space, we define the set of all gaits as

$$X = \{(x_0, t) \in \mathbb{R}^5 \mid G(x_0, t) - x_0 = 0\},$$



(a) part of a walking connected component



(b) part of a brachiating connected component

Figure 3.2. Parts of two connected components projected onto the q_2 - t plane. Every point is a gait in the state-time space. The cartoon animations are the swing motions at points A-E. The walking connected component has an infinite number of solutions [22] branching off the curve at $q_2 = 180^\circ$, while the brachiating curve does not have branching solutions.

where x_0 , t , and G are defined in Section 3.3. Let $S = (X, \mathcal{O} \cap X)$ be a subspace topology of the standard topology $T = (\mathbb{R}^5, \mathcal{O})$, where \mathcal{O} is the collection of open sets in \mathbb{R}^5 . By the implicit function theorem, if the Jacobian matrix

$$J(x_0^*, t^*) = \begin{bmatrix} \frac{\partial G}{\partial x_0} & \frac{\partial G}{\partial t} \end{bmatrix} (x_0^*, t^*) - \begin{bmatrix} \frac{\partial x_0}{\partial x_0} & \frac{\partial x_0}{\partial t} \end{bmatrix}$$

has maximal rank at a fixed point (x_0^*, t^*) , then nearby solutions form a 1-D curve passing through (x_0^*, t^*) in the state-time space. If $J(x_0^*, t^*)$ does not have maximal rank, then locally the nature of the connected component requires further analysis. It is at these fixed points where multiple 1-D curves can intersect. We trace the connected components of X using an Euler-Newton numerical continuation method. [2] There are many connected components in the 5-D state-time space. Figure 3.2 shows parts of two connected components projected onto a 2-D subspace of the state-time space. The connected component of walking gaits in Figure 3.2(a) is comprised of three 1-D curves glued together at two fixed points $([\pi, \pi, 0, 0]^T, 1.59)$ and $([\pi, \pi, 0, 0]^T, 1.78)$, where $J(x_0^*, t^*)$ is not maximal rank. The black, straight-line curve at $q_2 = 180^\circ$ consists of the state $[\pi, \pi, 0, 0]^T$ for all switching times t^* . The state is an equilibrium point of the double pendulum dynamics. For the connected component of brachiating gaits in Figure 3.2(b), $J(x_0^*, t^*)$ evaluated at every fixed point along the curve has maximal rank. Because of this, the curve has a unique arc-length parameterization. [60] There are other 1-D solution curves of brachiating gaits (see, e.g., Figure 3.4), but these curves are not connected to each other.

In the Introduction, we defined walking and brachiating based on whether the links cross or not. For a trajectory to be a fixed point, the angle of the swing leg must equal $q_2(t) = -q_2(0) = -q_2^*$ prior to impact. This puts a constraint on the net angular displacement of the swing leg

$$\Delta q_2 = \int_0^t \dot{q}_2(s) ds = 2\pi k - 2q_2^*,$$

where k is an integer. For $|\Delta q_2| \leq 2\pi$, the net angular displacement has the intuitive meaning of the links crossing or not crossing (Figure 3.3). If $q_2^* \in [-\pi, \pi]$,¹ then $k \in \{-1, 0, 1\}$, where $k = 0$ is a brachiating gait and $|k| = 1$ is a walking gait. We have

¹Removing $-\pi$ or π excludes brachiating either counterclockwise or clockwise at $q_2^* = \pi$.

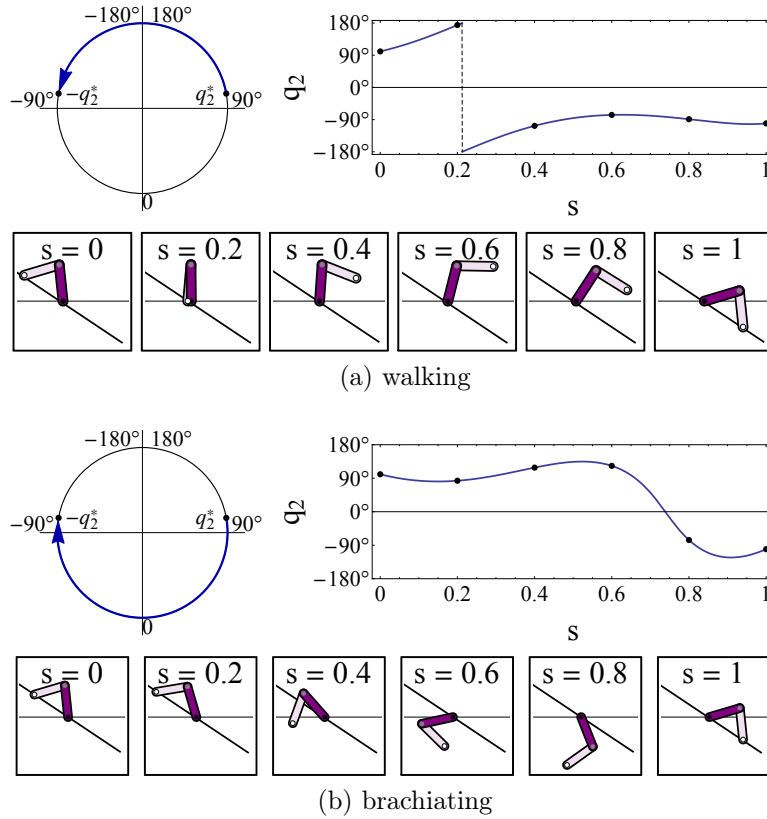


Figure 3.3. The trajectory of the swing leg of two gaits with the same initial configuration $q \approx (-174.1^\circ, 100.6^\circ)$ are shown. The arrow on the circle corresponds to the net displacement of the swing leg relative to the stance leg, the plot is the swing leg's trajectory scaled to each gait's switching time, and the animations are snapshots of the robot's trajectory over time. The net displacement of the walking gait (a) crosses 180° (i.e., the links cross), while the brachiating gait (b) crosses zero (i.e., the links did not cross).

now partitioned the set of fixed points into two sets. Let B and W be the set of fixed points with values of $|k|$ equal to 0 and 1, respectively. By construction, we have that $B \cup W = X$. If there is a continuous path between fixed points in B and W , then there must exist a fixed point on the path that is in both sets. Such a fixed point cannot exist, because this would mean that the same state has two different trajectories—one where the links cross and another where they do not. This cannot be true as solutions to the

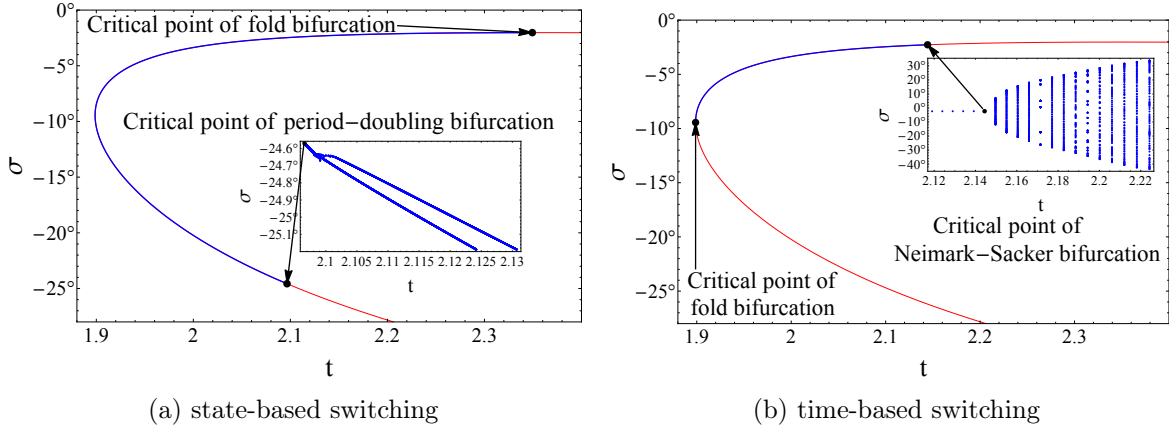


Figure 3.4. Stability of gaits on a brachiating solution curve under (a) state-based and (b) time-based impacts. The impacts can occur at a fixed slope σ or switching time t . The blue segments of the curve are stable fixed points and the red are unstable. The types of bifurcation are also highlighted. The insets show the higher period gaits that result.

differential equation of the double pendulum are unique. Hence, $B \cap W = \emptyset$ and no path can exist between gaits in these sets.

While a continuous path cannot exist between a walking gait and a brachiating gait, connected components in both B and W connect gaits that locomote above and below the surface. Figure 3.2(a) shows a path in W that continuously deforms a walking gait starting at the gait labeled B to what is often referred to as “over-hand” [21] brachiation (gait C). Topologically, this gait is equivalent to a gait that “walks” below the surface.

3.5. Stability and Bifurcations

The switching time t plays an interesting role in our model. If we treat it as a free parameter, then we can impact whenever we want. If instead the robot impacts when it returns back to its initial slope σ , then $t = t(x_0)$ is dependent on the state. Figure 3.4 shows the stability of a 1-D curve of brachiating gaits under the two switching strategies as we move along the curve (this curve does not intersect the curve in Figure 3.2(b), which does not have stable time-based gaits). In the example of Figure 3.4, the set of stable time-based switching gaits is a subset of the set of stable state-based switching gaits. In our experience, all gaits that are stable under time-based switching are also stable under

state-based switching, but the converse is not true. While both switching strategies give rise to fold bifurcations, we have also observed period-doubling bifurcations in the case of state-based switching and Neimark-Sacker bifurcations [42] in the case of time-based switching.

3.6. Discussion

We have presented results on the connected components and stability of gaits for a two-link robot capable of brachiating and walking using a generalized two-link model. We have shown that walking and brachiating are distinct gaits, but they are not differentiated by moving above or below a slope. We have also shown that the impact strategy affects the stability of a gait, where state-based impacts are more stable than time-based impacts.

For future work, we plan to extend our model to powered gaits in a state-control space that includes control parameters for an actuator at the joint. Do connected components remain disconnected in this higher-dimensional state-control space or are they part of the same connected component that appears disconnected when projected onto the 5-D state-time space of passive gaits studied in this paper?

CHAPTER 4

Stable Open-Loop Brachiation on a Vertical Wall

This chapter first is from [67]. Several authors contributed to the paper; I am the lead author. My primary results are in Section 4.6. The paper introduces the Gibbot, a brachiating two-link robot. The Gibbot was meant to serve as an experimental platform for studying hybrid dynamical systems with state- and time-based switching. Due to several design challenges, the experimental test bed was never fully realized. Ultimately, the main contribution of the Gibbot was as an educational learning tool for the large number undergraduates who were involved with the project. The contributions of this chapter to the thesis are

- (1) A canonical hybrid dynamical system with real-world applications, such as in search and rescue, structural monitoring (e.g., building, ships, and bridges [50]), and exploration [10],
- (2) The use of numerical continuation methods to generate families of gaits from Gomes-Ruina (GR) solutions [25] as motion templates. GR gaits are a class of swing motions that impact at zero velocity and perform zero work throughout the swing,
- (3) The generation of stable up and downhill gaits based on inherently unstable but extremely energy efficient motion templates, and
- (4) the ability to “grow” a connected component from a family of passive dynamic (i.e., unactuated) gaits to include a set of actuated gaits that can brachiate uphill.

4.1. Abstract

This paper presents a hybrid mechanical model for the Gibbot, a robot that dynamically locomotes along a vertical wall in a manner analogous to gibbons swinging between



Figure 4.1. The Gibbot executing a single brachiation swing on a steel wall.

branches in the forest canopy. We focus on one particular gait, continuous-contact brachiation, which always has one handhold in contact with the wall. We use zero-cost, unstable solutions corresponding to horizontal brachiation, originally found by Gomes and Ruina, as templates to generate open-loop stable gaits in arbitrary directions. The first case considered is passive brachiation down a shallow slope, roughly corresponding to upside-down locomotion of the well-studied compass-gait biped. We then consider underactuated brachiation with a constant forcing term at the elbow to produce open-loop stable descending and ascending gaits.

4.2. Introduction

This paper introduces the Gibbot, a dynamic climbing robot developed for experimental validation of estimation and control of hybrid mechanical locomotion systems. The Gibbot locomotes on a vertical wall and consists of two links, each equipped with a “hand,” and a single powered rotary joint connecting the two links. A hand can clamp to the wall at any time, with the link freely pivoting about the clamp. The robot locomotes by actuating the joint motor and switching between four dynamic regimes: one hand clamped, the other hand clamped, both hands free (free flight), or both hands clamped (rendering the Gibbot stationary). Our Gibbot prototype climbs on a steel wall, so we use electromagnets mounted in rotary bearings to implement the hand clamping mechanism. Due to the availability of “handholds” at any location on the wall, the Gibbot is capable of a wide variety of gaits, each consisting of a cyclic sequence of transitions among these regimes.

In this paper we focus on one particular gait of the Gibbot: continuous-contact brachiation (Figure 4.1). Brachiation is the style of locomotion employed by gibbons (from which the Gibbot draws its name) as they gracefully locomote through the forest canopy

by swinging between branches. Fukuda and colleagues introduced brachiation to robotics by building a series of robots demonstrating the ability to swing from handhold to handhold in gravity [21, 54, 72]. The earliest brachiating robots consisted of two links with grippers and a single powered rotary joint, similar to the Gibbot in this paper, while later versions consisted of many degrees of freedom to better approximate the articulation of a gibbon.

The Gibbot differs from hybrid systems such as the brachiation robots of Fukuda et al., as well as walking robots, in that regime jumps can be implemented at arbitrary states. This ability to activate and deactivate the clamps at any time allows the exploration of a wide variety of gaits without the need for precisely placed handholds.

4.2.1. Statement of Contributions

This paper introduces the design of the Gibbot and demonstrates its operation. We then focus on brachiation by the Gibbot, motivated by the observation by Gomes and Ruina that zero-energy horizontal brachiation is theoretically possible [25]. They showed that, for certain initial rest configurations of the two-joint robot, and assuming zero damping or friction, the swing-through hand reaches a horizontal line of handholds with the robot at zero velocity and in a mirrored configuration of the original. This allows the robot to release one hand and clamp the other, which requires zero work, and resume swinging.

These fixed-point solutions of the dynamics consume zero energy, but they are unstable and apply only to horizontal locomotion. Using these motions as templates, in this paper we extend these solutions to “nearby” *stable* brachiation gaits:

- **Unactuated downhill brachiation.** We show the existence of stable downhill brachiation solutions without powering the motor. The swing-through hand clamps on the downhill slope at nonzero velocity, causing an energy-dissipating impact. Potential energy due to gravity restores the kinetic energy by the end of the next swing, resulting in a fixed point in the dynamics. For some slopes, these fixed points are shown to be stable. The passive brachiator is roughly analogous

to an upside-down passive compass gait walker [22, 26], but the brachiator has gaits with much larger domains of attraction.

- **Open-loop brachiation in arbitrary directions.** We show the existence of stable powered brachiation gaits without the use of feedback. Certain choices of swing-through duration and actuator torques lead to stable fixed points corresponding to horizontal brachiation, uphill brachiation, and downhill brachiation.

This general strategy of morphing unstable passive dynamic motions into powered but stable motions leads naturally to graceful locomotion, typically with a trade-off between stability and efficiency.

4.2.2. Related Work

The work reported in this paper has two main inspirations: the brachiation robots of [21, 54, 72] and the theoretical zero-energy horizontal brachiation of [25]. Brachiation on isolated handholds is achieved by feedback control in [21, 54, 72], while our focus is on unactuated and open-loop control. Unstable zero-energy brachiation is studied in [25]; in this paper, we focus on nearby energy-efficient but stable brachiation gaits.

The approach of using zero-energy locomotion solutions as templates for controlled solutions has been employed by Ruina et al. for nearly-passive controlled walking on flat ground [18] and Spong et al. for walking on varying slopes [76] and in 3D spaces [28].

Other robots which share a family resemblance to the Gibbot are the two-link robot of Bullo and Žefran [11], the Acrobot [75], the ROCR robot of Provancher et al. [61], and the bridge inspection robot of Mazumdar and Asada [50]. The two-link hybrid robot described in simulation in [11] locomotes on a horizontal plane by switching between sliding, clamped, and rolling modes, and is used to demonstrate controllability properties of hybrid mechanical systems. When the Gibbot has a single hand clamped, it becomes the Acrobot [75], a double pendulum with an actuator at the middle joint. The use of clamping and dynamic swinging motions for climbing locomotion is also employed in ROCR, which uses claws to grasp a textured wall [61]. The bridge inspection robot



Figure 4.2. (Top) Perspective view of the Gibbot. (Bottom) A view of the underside of the Gibbot.

in [50] uses intermittent brachiation-style swinging motions to “step over” obstacles on the underside of a bridge, but the robot must come to rest between steps.

The Gibbot’s hand clamping mechanism uses an electromagnet mounted in rotary bearings. This choice was made for design simplicity and fast activation/deactivation of the clamps, but not for power efficiency. Another option for activating and deactivating a clamp is to mechanically rotate a permanent magnet [50, 64], which has the advantage that no power is needed to maintain the clamp indefinitely, at the possible cost of speed of attachment and detachment.

4.2.3. Paper Outline

We begin in Section II by describing the design and operation of the Gibbot. Section III provides a mathematical model of the hybrid mechanical system and summarizes the results of Gomes and Ruina [25]. Section IV examines passive downhill brachiation, and Section V addresses open-loop stable powered brachiation on arbitrary slopes. We conclude in Section VII with remarks and future work.

4.3. Gibbot Design and Operation

The Gibbot began as an undergraduate mechatronics project and has evolved to the current design, built in collaboration with Kinea Design, LLC (Figure 4.2). The robot locomotes on a vertical steel sheet by switching its two electromagnets on and off and powering the motor at its middle joint. A geared 19.5:1 GM8224 Pittman motor with

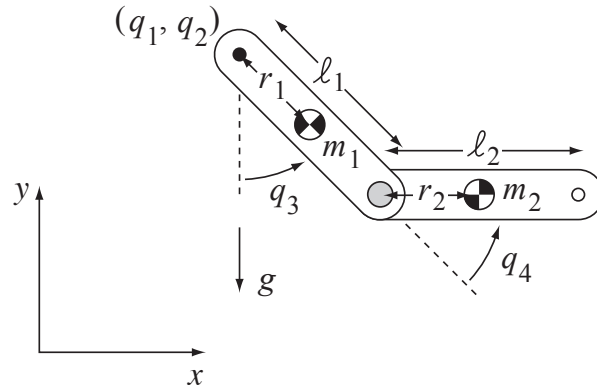


Figure 4.3. The Gibbot model.

a 500 line encoder powers the elbow joint. An additional 3:1 bevel gearing allows the motor to lay flat along one link and brings the maximum output torque at the joint to approximately 6 Nm. The electronics of the robot consist of an onboard PIC32 running at 80 MHz with an XBee chip for wireless communication. In addition to the motor encoder, the Gibbot is outfitted with two rotary encoders mounted over the magnets, as well as gyros and accelerometers on each link to measure the angular velocity and acceleration of the arms. Three LEDs are visible to an external high-speed camera, allowing real-time feedback control over the wireless XBee link. The entire robot is powered by two 11.1 V Lithium-ion batteries. The total weight of the robot is about 2.36 kg. We have included a supplementary video of the Gibbot in motion available at <http://ieeexplore.ieee.org>.

4.4. The Hybrid Dynamics

Notation for the Gibbot is shown in Figure 4.3. The configuration vector is written $q = [q_1, q_2, q_3, q_4]^T$, where (q_1, q_2) are the x - y coordinates of hand 1 in a world frame, q_3 is the angle of link 1 from the vertical, and q_4 is the angle of link 2 from link 1. The lengths of the two links from the hands to the motor are l_1 and l_2 , and r_1 and r_2 are the distances from the hand to the center of mass of link 1 and from the motor to the center of mass of link 2, respectively. The mass and inertia of the links about their center of mass are m_i and I_i .

Magnet State	Magnet 1	Magnet 2	Dynamics
0	0	0	Free Flight
1	0	1	Double Pendulum
2	1	0	Double Pendulum
3	1	1	At Rest

Table 4.1. Four magnet states and corresponding motions.

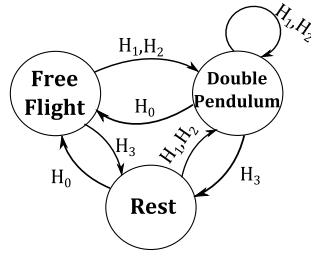


Figure 4.4. The hybrid dynamics as a finite state machine.

The Gibbot is a hybrid mechanical system described by four different dynamic regimes (free flight, hand 1 clamped, hand 2 clamped, or both hands clamped) depending on the on-off state of the two magnets. We represent the magnet state as $b \in \{0, 1, 2, 3\}$ (Table 4.1). Two of these regimes correspond to double pendulum dynamics, so we collapse them into one in the finite state machine of Figure 4.4. The hybrid dynamics consists of periods of motion within a regime punctuated by transitions between regimes, which may result in instantaneous change of the Gibbot velocity. Defining $x = [q^T, \dot{q}^T]^T$ as the state of the system, a transition between regimes is represented by

$$x^+ = H_{b^+}(x^-),$$

where x^- is the pre-transition state, x^+ is the post-transition state, and b^+ is the post-transition regime. Thus there are four transition maps, H_0 through H_3 , depending on the hand state after the jump.

Below we give the continuous dynamics within the regimes, then the transition maps due to changing magnet states, and finally define fixed points of the hybrid dynamics and the zero-energy fixed points discovered by Gomes and Ruina.

4.4.1. The Continuous Dynamics

We nondimensionalize the dynamics such that time is scaled by $d_t = \sqrt{\frac{\ell_1 + \ell_2}{g}}$, lengths are scaled by $d_\ell = \ell_1 + \ell_2$, and torques are scaled by $d_u = gm_2r_2$. This results in the following set of nondimensionalized parameters used in this section:

$$\begin{aligned}\alpha &= d_\ell \frac{m_1 + m_2}{m_2 r_2} & \beta &= \frac{m_1 r_1 + m_2 \ell_1}{m_2 r_2} \\ \delta_1 &= \frac{\ell_1}{d_\ell} & \delta_2 &= \frac{\ell_2}{d_\ell} \\ \gamma &= \frac{g d_t^2}{d_\ell} & \kappa_1 &= \frac{1}{d_\ell} \left(\frac{I_2}{m_2 r_2} + r_2 \right) \\ \kappa_2 &= \frac{1}{d_\ell} \left(\frac{I_1 + m_1 r_1^2}{m_2 r_2} + \frac{\ell_1^2}{r_2} \right)\end{aligned}$$

4.4.1.1. The Free Flight Dynamics, Regime 0. If both magnets are off, then the robot is in free flight and the equations of motion are

$$(4.1) \quad \dot{x} = \begin{bmatrix} \dot{q} \\ M_0^{-1}(q)(U_0 - C_0(q, \dot{q})\dot{q} - G_0(q)) \end{bmatrix},$$

where U_0 is the control vector, M_0 is the inertia matrix, C_0 is the Coriolis matrix, and G_0 is the gravitational vector:

$$(4.2) \quad \begin{aligned}U_0 &= \gamma \begin{bmatrix} 0 \\ 0 \\ 0 \\ u \end{bmatrix} \\ M_0(q) &= \begin{bmatrix} \alpha & 0 & \beta c_{34} + c_{34} & c_{34} \\ 0 & \alpha & \beta s_{34} + s_{34} & s_{34} \\ \beta c_{34} + c_{34} & \beta s_{34} + s_{34} & \kappa_1 + \kappa_2 + 2\delta_1 c_4 & \kappa_1 + \delta_1 c_4 \\ c_{34} & s_{34} & \kappa_1 + \delta_1 c_4 & \kappa_1 \end{bmatrix} \\ C_0(q, \dot{q}) &= \begin{bmatrix} 0 & 0 & -(\beta s_3 \dot{q}_3 + s_{34}(\dot{q}_3 + \dot{q}_4)) & -s_{34}(\dot{q}_3 + \dot{q}_4) \\ 0 & 0 & \beta c_3 \dot{q}_3 + c_{34}(\dot{q}_3 + \dot{q}_4) & c_{34}(\dot{q}_3 + \dot{q}_4) \\ 0 & 0 & -\delta_1 s_4 \dot{q}_4 & -\delta_1 s_4(\dot{q}_3 + \dot{q}_4) \\ 0 & 0 & \delta_1 s_4 \dot{q}_3 & 0 \end{bmatrix} \\ G_0(q) &= \gamma \begin{bmatrix} 0 \\ \alpha \\ \beta s_{34} + s_{34} \\ s_{34} \end{bmatrix}.\end{aligned}$$

We use the short-hand notation c_{34} to denote $\cos(q_3 + q_4)$ and similarly for the sine function.

4.4.1.2. The Double Pendulum Dynamics, Regimes 1 and 2. If only one magnet is on, then the Gibbot swings like a double pendulum. Defining (q_1, q_2) to be the pivot point, we focus on a reduced set of coordinates (q_3, q_4) , known as the shape variables.

Defining $\theta = [q_3, q_4]^T$, the reduced set of equations are

$$(4.3) \quad \ddot{\theta} = M_1(\theta)^{-1}(U_1 - C_1(\theta, \dot{\theta})\dot{\theta} - G_1(\theta)),$$

where

$$(4.4) \quad \begin{aligned} U_1 &= \gamma \begin{bmatrix} 0 \\ u \end{bmatrix} \\ M_1(\theta) &= \begin{bmatrix} \kappa_1 + \kappa_2 + 2\delta_1 c_4 & \kappa_1 + \delta_1 c_4 \\ \kappa_1 + \delta_1 c_4 & \kappa_1 \end{bmatrix} \\ C_1(\theta, \dot{\theta}) &= \begin{bmatrix} -\delta_1 s_4 \dot{q}_4 & -\delta_1 s_4 (\dot{q}_3 + \dot{q}_4) \\ \delta_1 s_4 \dot{q}_3 & 0 \end{bmatrix} \\ G_1(\theta) &= \gamma \begin{bmatrix} \beta s_3 + s_{34} \\ s_{34} \end{bmatrix}. \end{aligned}$$

4.4.1.3. The Rest Dynamics, Regime 3. When both magnets are on the robot cannot move, i.e., $\dot{x} = 0$.

4.4.2. The Transition Maps

In order for the robot to transition from one regime into the next, it has to change its magnet state. This may cause a jump in the velocity of the system. We capture this behavior with a transition map that sends the robot's state into a different dynamic regime. The transition map depends only on the new regime b^+ .

4.4.2.1. Transition to the Double Pendulum. When the robot transitions from free flight into double pendulum mode, or from one double pendulum mode to the other, the robot undergoes an impact at the magnet that turns on. This causes a jump in the velocity of the system.

We can relate the pre-impact velocities to the post-impact velocities using impulse and conservation equations, which give us an impact map $P(q)$. We assume that the impact is plastic, instantaneous, and that non-impulsive forces are negligible. This leads to the following set of equations:

$$(4.5) \quad q^+ = q^-$$

$$(4.6) \quad J(q^-)\dot{q}^+ = 0$$

$$(4.7) \quad M(q^-)(\dot{q}^+ - \dot{q}^-) = J^T(q^-) \Pi$$

where the $+$ and $-$ superscripts represent the pre- and post-impact variables, $M(q)$ is the mass matrix from the free flight dynamics, Π is the 2×1 impulse vector, and $J(q)$ is the Jacobian satisfying $\dot{p} = J(q)\dot{q}$, where \dot{p} is the linear velocity of the hand about to clamp. The first two equations are the instantaneous and plastic impact assumptions, while the third equation is the impulse and conservation equations in generalized coordinates. We now derive an expression for $P(q)$ by first rewriting (4.7) as

$$(4.8) \quad \dot{q}^+ = M^{-1}J^T\Pi + \dot{q}^-.$$

Substituting into (4.6) and rearranging terms, we get

$$\Pi = - (JM^{-1}J^T)^{-1} J\dot{q}^-.$$

Plugging the results back into (4.8), we arrive at

$$\dot{q}^+ = \left(I - M^{-1}J^T (JM^{-1}J^T)^{-1} J \right) \dot{q}^-$$

and define $P(q)$ as

$$(4.9) \quad P(q) = I - M(q)^{-1}J^T(q) (J(q)M(q)^{-1}J^T(q))^{-1} J(q).$$

Depending on which magnet is about to clamp, $J(q)$ can take one of two possible forms,

$$(4.10) \quad J_1(q) = \begin{bmatrix} 1 & 0 & 0 & 0 \\ 0 & 1 & 0 & 0 \end{bmatrix}$$

or

$$(4.11) \quad J_2(q) = \begin{bmatrix} 1 & 0 & \delta_1 c_3 + \delta_2 c_{34} & \delta_2 c_{34} \\ 0 & 1 & \delta_1 s_3 + \delta_2 s_{34} & \delta_2 s_{34} \end{bmatrix}.$$

We want to retain the same double pendulum dynamics regardless of whether J equals J_1 or J_2 , so there will be times when we need to redefine coordinates (i.e., which hand location is identified with (q_1, q_2)). We will write the jump map in such a way that the post-impact velocities are correct regardless of whether or not the coordinate system has

to be flipped. Let

$$(4.12) \quad A(q) = \begin{bmatrix} q_1 + \delta_1 s_3 + \delta_2 s_{34} \\ q_2 - \delta_1 c_3 - \delta_2 c_{34} \\ \pi + q_3 + q_4 \\ -q_4 \end{bmatrix},$$

which we will invoke whenever we need to flip the coordinate system. We also assume that the physical parameters and the labels for each link are swapped as well. Then the transition map is written

$$(4.13) \quad x^+ = H_i(x^-) = \begin{cases} \begin{bmatrix} q^- \\ P(q^-)\dot{q}^- \end{bmatrix}, & J = J_1 \\ \begin{bmatrix} A(q^-) \\ \frac{\partial A(q)}{\partial q}(q^-)P(q^-)\dot{q}^- \end{bmatrix}, & J = J_2 \end{cases}$$

for $i = 1, 2$.

4.4.2.2. Transition to Free Flight. Because there are no impulsive forces, the transition map is $x^+ = H_0(x^-) = x^-$.

4.4.2.3. Transition to Rest. When both magnets are activated the Gibbot becomes immobile, so we have

$$(4.14) \quad x^+ = H_3(x^-) = \begin{bmatrix} I & 0 \\ 0 & 0 \end{bmatrix} x^-.$$

4.4.3. Definition of a Brachiation Fixed Point

To draw a connection to the results of Gomes and Ruina, for the rest of the paper we assume the Gibbot is symmetric, so all masses, lengths, etc. of the two links are identical.

If we let b^+, b^- represent the pre- and post-impact magnet states, F_0, F_1, F_3 be the equations of motion of the free flight dynamics, double pendulum, and rest dynamics, respectively, and let $F_2 = F_1$ (by the symmetry of the Gibbot), then we can write the

dynamics from one post-transition state to the next as

$$(4.15) \quad x^+ = H_{b^+}(x^-) = H_{b^+} \left(x_0 + \int_0^T F_{b^-}(x(s), u(s)) ds \right)$$

and explicitly show the dependence on initial conditions x_0 , forcing function $u(t)$, switching time T , and magnet states b^+ and b^- . Defining λ as the collection of the switch time T , the new magnet state b^+ , and the control function $u(t)$, we can write (4.15) as $x^+ = \mathcal{H}(x_0, \lambda)$. If we restrict the robot's locomotion so that it is never in free flight, then we can define a return map S on the shape space with reduced state vector $x_\theta = [\theta^T, \dot{\theta}^T]^T$,

$$(4.16) \quad x_\theta^1 = S(x_\theta^0, \lambda^0).$$

Since the robot cannot be in free flight, the shape variables and their derivatives are sufficient to define a fixed point of the system corresponding to period-one cyclic motion, i.e.,

$$(4.17) \quad x_\theta^* = S(x_\theta^*, \lambda^*).$$

We define a brachiation fixed point as a solution (x_θ^*, λ^*) to (4.17) such that b^+ corresponds to the double pendulum mode.

4.4.4. The Gomes-Ruina Fixed Points

Some solutions of (4.17) do not require any torque throughout the swing motion. A subset of these solutions impact with zero velocity at time T^* in a configuration mirroring the original stationary configuration. These are the zero-energy horizontal brachiation fixed points identified for the symmetric brachiator by Gomes and Ruina (Figure 4.5). These solutions are fully specified by q_3^* , T^* , and zero control torque. We refer to these fixed points as Gomes-Ruina fixed points (or GR fixed points). An important consequence of zero impact velocity and zero energy input is that all GR fixed points are unstable. In the next section we explore stable fixed points of (4.16) that have non-zero velocity impacts. In our search for stable gaits, we used the same physical parameters used by Gomes and Ruina for their two link brachiator model. The nondimensionalized parameters for their

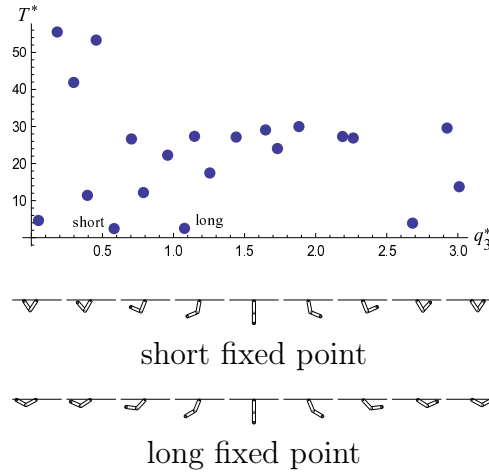


Figure 4.5. Several Gomes-Ruina fixed points in the (q_3^*, T^*) plane, and two solutions shown as animations.

system are approximately

$$\begin{aligned} \alpha &= 38.263 & \beta &= 18.132 & \delta_1 &= 0.5 & \delta_2 &= 0.5 \\ \gamma &= 1 & \kappa_1 &= 0.277 & \kappa_2 &= 8.843. \end{aligned}$$

4.5. Passive Downhill Brachiation

The GR solutions are unstable, as energy dissipation is necessary for stability. For periodic motion, this energy must be replenished. By brachiating downhill, similar to an upside-down compass gait walker [22, 26], in each cycle the Gibbot converts some potential energy to kinetic energy, and then dissipates the same amount of energy on impact. To create this downhill brachiation, we switch the magnets when the hands lie on a sloped line as seen in Figure 4.6. The slope that the Gibbot brachiates on has an angle $\sigma > 0$ from the slope to the horizontal.

We would like to find the stable and unstable period-one fixed points for passive downhill brachiation. These post-impact fixed points lie in a four-dimensional $(\sigma, q_4, \dot{q}_3, \dot{q}_4)$ space. (Note that the slope angle σ and q_4 uniquely define q_3 just after impact.) We will find it convenient to represent the post-impact configuration on the slope by the *interleg angle* $\nu = \pi - q_4$, illustrated in Figure 4.6. Thus our search for fixed points is in the four-dimensional $(\sigma, \nu, \dot{q}_3, \dot{\nu})$ space, which we call \mathcal{M} .

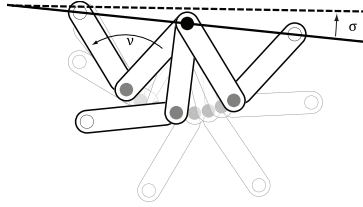


Figure 4.6. An example of passive stable downhill brachiation on a slope of $\sigma = 0.1$ radians and an interleg angle of $\nu = 1.287$ radians.

The unstable “short” and “long” GR solutions, illustrated in Figure 4.5, are isolated points in the four-dimensional space \mathcal{M} , at $\nu = 1.16$ radians for the short solution, $\nu = 2.15$ radians for the long solution, and $\sigma = \dot{q}_3 = \dot{\nu} = 0$ for both. The idea is to use these solutions as starting points and apply continuation methods to search for the existence of nearby fixed points in \mathcal{M} where $\sigma > 0$, corresponding to downhill brachiation. (There can be no passive fixed points for $\sigma < 0$; actuated, but open-loop, fixed points are considered in Section 4.6. These two GR solutions are the shortest-duration and simplest brachiation motions, and therefore the most likely prototypes for stable open-loop uphill brachiation.) We limit our study to a neighborhood of these two solutions and do not attempt to fully understand the topology of the fixed points in \mathcal{M} . See Figure 4.5 for an idea of the complexity.

Our results are summarized in Figure 4.7, which is a projection of \mathcal{M} onto the (σ, ν) space. The projections of the GR solutions are indicated by asterisks. Starting from the unstable long GR solution, we increase σ slightly to $\sigma + \delta$ and use an optimization-based continuation method to find a nearby point $(\sigma + \delta, \nu, \dot{q}_3, \dot{\nu})$ satisfying the fixed-point condition (4.17). This new point is the initial guess to find a next fixed point at $\sigma + 2\delta$, etc. This method shows that the long GR solution belongs to a one-dimensional family of fixed points extending to downhill slopes up to approximately $\sigma = 0.14$ radians, or 8 degrees. This family is denoted A in Figure 4.7. These fixed points are stable in the range $0.005 < \sigma < 0.128$.

We also found a family B of unstable fixed points running from slopes of approximately $\sigma = 0.01$ radians to $\sigma = 0.43$ radians. This family appears to connect to the short GR solution, but we were unable to verify this definitively.

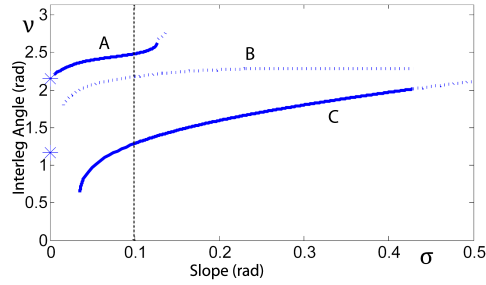


Figure 4.7. Fixed-point families A, B, and C projected to (σ, ν) . Solid lines indicate stable fixed points and dashed lines indicate unstable. Asterisks at zero slope indicate GR solutions. The dotted vertical line at a slope of 0.1 radians indicates the slice shown in Figure 4.9.

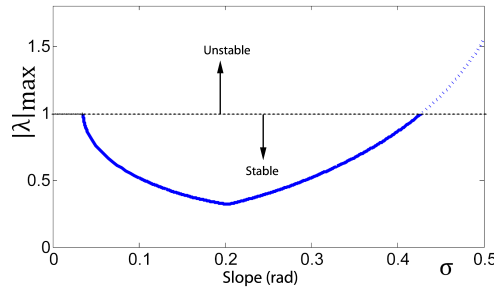


Figure 4.8. The magnitude of the largest eigenvalue of the return map S of family C fixed points, plotted as a function of slope.

Finally, we found one other nearby solution family C that does not appear to be connected to a GR fixed point. This family C extends from $\sigma = 0.035$ radians to beyond $\sigma = 0.5$ radians, and includes stable fixed points from $\sigma = 0.035$ radians to $\sigma = 0.435$ radians.

Figure 4.8 plots the magnitude of the maximum eigenvalue of the return map S corresponding to points in family C. According to this measure, passive downhill brachiation is most stable at a slope of $\sigma = 0.2$.

Figure 4.9 plots the basins of attraction of the family A “long” interleg angle stable fixed points and the family C “short” stable fixed points in the two-dimensional slice $\{\mathcal{M} \mid \sigma = 0.1, \dot{q}_3 = 0\}$. Each point in this slice converges to a stable A or C fixed point. Thus the basins of attraction of the two stable fixed-point families are quite large (and

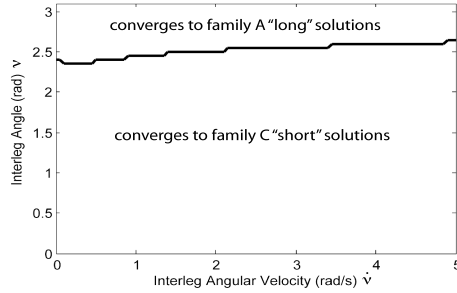


Figure 4.9. Basins of attraction for family A and family C stable fixed points for a slope of $\sigma = 0.1$ radians and $\dot{q}_3 = 0$.

appear to partition the entire $(\nu, \dot{\nu})$ space), unlike the fixed points of the Gibbot’s inverted counterpart, the compass-gait walker. Also unlike the compass-gait walker, we did not observe period-doubling bifurcations in brachiation gaits at steep slopes where the stable period-one solutions disappear.

Because of the large basins of attraction of the stable fixed points of families A and C, these fixed points are easy to find through simulation. Our simulations confirm that the stable fixed points are disconnected one-dimensional curves in \mathcal{M} . For all initial conditions we tried, the Gibbot converged either to a stable point in A, a stable point in C, or never converged at all. We did not observe other periodic or quasi-periodic gaits.

By a counting argument, we hypothesize that the families A, B, and C, including the unstable fixed points, are one-dimensional sets. The fixed-point condition places three constraints on the four variables in \mathcal{M} , generically resulting in one-dimensional solution sets. Figure 4.9 is indicative of a three-dimensional unstable surface separating families A and C, which we see as a line in the projection of the figure.

Finally, by analogy to the compass-gait walker, in this section we assumed that the free-swinging magnet activates upon reaching the virtual slope. While this happens mechanically for the walker, the Gibbot requires a sensor to implement this switch. To eliminate this sensor, we also considered the case where the Gibbot switches the magnets according to a time schedule. Preliminary tests show that stable solutions shown above

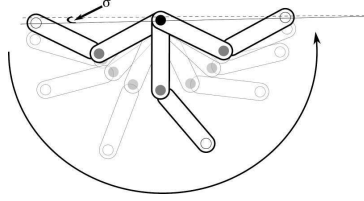


Figure 4.10. An example of an actuated uphill brachiation on a slope of 0.024 radians.

remain stable under this alternate time-based switching strategy. Thus passive downhill brachiation can be both stable and sensorless. In the next section, we investigate a time-based switching strategy for powered, but still sensorless, uphill brachiation.

4.6. Uphill Stable Brachiation

One limitation of the passive brachiating solutions is that the continuous contact gaits can only brachiate downhill. We can overcome this limitation by powering the motor for which we choose the simplest forcing function, $u(t) = u > 0$. An example of an uphill brachiating fixed point is shown in Figure 4.10. This particular fixed point is part of a family of uphill climbing solutions that extend from the long GR solution, which has an initial configuration of $(q_3^*, q_4^*) \approx (-1.077, -0.987)$ and switching time $T^* \approx 2.508$. The initial condition x_θ^* , torque u^* , and switching time T^* for the uphill climbing gait are approximately

$$(4.18) \quad \begin{aligned} x_\theta^* &= \left[-1.065, \quad -0.964, \quad 0.044, \quad -0.007 \right]^T, \\ u^* &= 0.451, \quad T^* = 2.514. \end{aligned}$$

The fixed point is stable (as illustrated in Figure 4.11) with a maximum eigenvalue of about 0.95. In our numerical simulations we find several families of fixed points parametrized by the controls, where the special case of $u = 0$ corresponds to a Gomes Ruina solution. Unlike the GR solutions, our climbing solutions are sometimes stable, and unlike existing control strategies for brachiation that we have found in the literature, our method is open-loop.

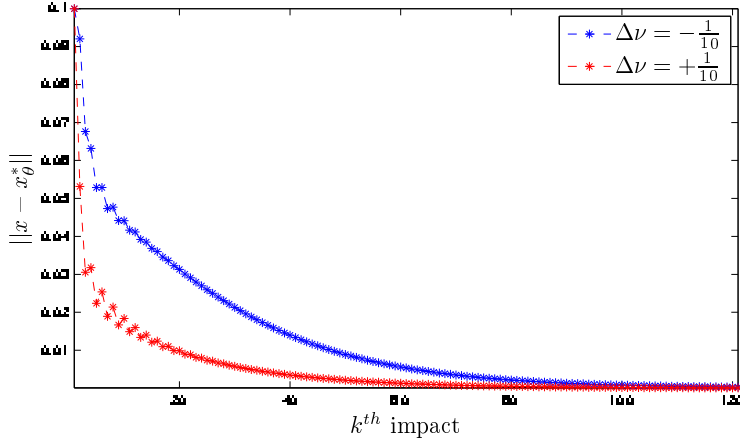


Figure 4.11. The normed error between the uphill fixed point and the post-impact state due to small perturbations of $\pm\frac{1}{10}$ radian to the interleg angle ν at $t = 0$.

In our simulations we have found stable downhill and uphill motions of varying periodicity, but with only one torque and switching time for controls we are limited in the nearby fixed points we can reach from a GR solution. We can show that if we break $u(t)$ into a piecewise-constant function comprised of three constant torques that, along with the final switching time, we can locally reach a full dimensional subset of fixed points near a GR solution. Because of space constraints we cannot show the derivation, but in future work we plan to utilize the result for planning more complicated motions besides the ones presented in this paper.

4.7. Discussion

We have shown that unstable, zero-energy brachiating solutions serve as natural templates for stable brachiation with or without control. In a future paper, we plan to expand on our numerical results. For example, our simulations show that the long Gomes-Ruina solution was capable of producing stable locomotion for passive descent and controlled ascent, i.e., open-loop control destabilized the passive gait. Controlled descent was the only stable locomotion produced by the short solution, i.e., open-loop control stabilized the unstable passive motion. These results suggest that the long zero-energy solution is

more useful as a motion template for brachiating in arbitrary directions. Future work will verify these observations experimentally.

We noticed several differences between passive brachiation and previous results on passive walking. We found two families of stable brachiating solutions over a range of slope angles, whereas only one family of stable walking solutions has been reported in the literature [22, 26]. Neither stable family exhibited period-doubling behavior on extreme slope angles, whereas a period-doubling cascade into chaos has been documented for the compass-gait biped [26]. Although this paper did not examine regions of attraction in-depth, the stable brachiating gaits were attractive for a large range of initial conditions. This suggests that the region of attraction for passive brachiating may be significantly larger than for passive walking, which is known to be sensitive to initial conditions. We leave this robustness analysis to future work.

This paper motivates further study of the Gibbot, which is capable of other forms of locomotion. Our model can transition into free-flight dynamics during swing phase to allow fast *ricochetal* brachiation. We are also interested in analyzing period-two (asymmetric) locomotor patterns. By employing a diverse suite of gaits, the Gibbot will be able to perform gymnastic maneuvers to reach specific handholds in the environment. Future work will use motion planning approaches based on asymptotically stable primitives [27] or optimization [47] to generate paths composed of these dynamic motions.

CHAPTER 5

Conclusion

We have presented a topological approach to gait generation for a class of biped robots that are physically symmetric with point, curved, and flat feet. In this thesis, we search for gaits in a parameterized space of trajectories $\mathcal{S} = \mathcal{X} \times \mathbb{R} \times \mathcal{M}$ consisting of a pre-impact state $x_0 \in \mathcal{X} \subseteq \mathbb{R}^{2n}$, a switching time $\tau \in \mathbb{R}$ and a vector of input parameters $\mu \in \mathcal{M} \subseteq \mathbb{R}^k$ that parameterize a family of trajectories $x(\tau) = \varphi_\mu^\tau(x_0) \in \mathcal{X}$ that satisfy a biped's (fixed-switching-time-based) hybrid dynamics. In \mathcal{S} , we are interested in the gait space $\mathcal{G} = P^{-1}(0)$, which represents the set of all gaits in \mathcal{S} . The zeros of P , $P(c) = \varphi_\mu^\tau(x_0) - x_0 = 0$, correspond to fixed points of the hybrid dynamics. The task is to find a path $p : \mathbb{R} \rightarrow \mathcal{G}$ starting from an equilibrium gait $c_{\text{eq}} \in E$ and ending at the footstep of a subset of gaits $\mathcal{G} - E$. At which point, we can begin to construct the set $\mathcal{G}_{\text{mapped}}$, which consists of gaits that can locomote in their environment.

Using a representative set of biped models found in the literature, we have generated a family of gaits (i.e., connected components) for bipeds that brachiate and walk based on their respective equilibrium points. In particular, we have presented the theory and algorithms behind generating these connected components. For biped robots, this includes gaits that are completely unactuated (passive dynamic walking gaits) and gaits that are subject to virtual holonomic constraints (constraints that are enforced using feedback control).

5.1. Future Work

While we have shown that our approach works on a variety of biped models, what this body of work is missing that is crucial to show the effectiveness of this technique is an experimental results on a real robot. We are curious to find out how quickly the

computations can be performed on an actual platform where we can incorporate sensor information.

With respect to software, while all of the models presented in this thesis use an adaptive step-size integrator (using Mathematica’s NDSolve), we would like to have extended our fixed step integration routines as well in order to directly compare our algorithms to direct collocation methods used in the literature [36, 58]. In particular, we would like to include implicit time-stepping algorithms as in [79] in a way that we could also automatically differentiate these computational steps using our internally developed algorithmic differentiator [66]. Another direction for future work is implementing more established optimization routines in finding desired gaits on the manifold, for example, a modified Nelder-Meade algorithm that operates on the connected component. A benefit of this type of solver is that we can attempt to find stable gaits using a derivative-free approach [52]. We could also compare other solvers to the Global Homotopy Map.

For future work, there are several interesting open topological and differential geometric questions that arise from our framework. In our work, we define a gait as a fixed point of the robot’s hybrid dynamics. These fixed points form connected components in a state-time-control space \mathcal{S} . Questions that we plan to explore in the future are:

- **Can all connected components of a given biped model be enumerated?** For a generalized two-link model with symmetric links, we have been able to make some progress for the specific case of the biped’s passive gaits [65]. In this model, we know that there exists at least two sets of passive gaits. We also know that it is not possible to reach all passive gaits of the two-link model from equilibria. In future work, we want to generalize these results to multi-degree-of-freedom biped models.
- **How many and what type of controls are necessary to make every state in the biped’s state space \mathcal{X} into a fixed point?** If every state in the state-time-control space can be made into a fixed point, then we have a surjective mapping from our controls subspace to the state subspace. This mapping can be useful for planning and control algorithms. For an underactuated two-link

robot, we can show that locally a piece-wise constant function made up of three constants is sufficient. We are working on the generalized problem.

- **How do we incorporate feedback control into our framework?** We want to design feedback controllers so that 1) every gait in a target connected component is stable, or 2) the manifold of gaits is attractive in the state-time-control space. The use of VHCs in our framework is an important first step in this direction.
- **How does the switching strategy used to trigger an impact affect the gaits of a connected component?** We are interested in studying the effect of open-loop stability of a gait based on *time-based* switching (impacts occur after a set period of time has elapsed) and *state-based* switching (impacts occur based on the robot's state, for example, when the swing leg collides with a predefined walking surface). We show preliminary results in [65] for walking and brachiating gaits of a generalized two-link biped.

As a final direction for future work, the key ingredients of our framework are

- a known point on a connected component that contains walking gaits,
- a method for tracing branches on the connected component, and
- a method for detecting and switching to different branches on the connected component.

This high-level description of our framework may lead to continuation methods being applied to areas outside of bipedal locomotion. Despite using language specific to biped walkers, our description of the approach in Section 2.4.1 can be generalized. We expect our approach to be applicable to other areas of robotics where a simple task (such as walking) can be continuously deformed into a more complicated task. An obvious next step is to extend our work to running bipedal robots or more general polypedal robotic system.

References

- [1] F. Aghili. A unified approach for inverse and direct dynamics of constrained multi-body systems based on linear projection operator: Applications to control and simulation. *IEEE Trans. on Robotics*, 21(5):834–849, 2005.
- [2] E. Allgower and K. Georg. *Numerical Continuation Methods, An Introduction*. Springer-Verlag New York, Inc., New York, NY, 1990.
- [3] Drumi Bainov and Pavel Simeonov. *Impulsive Differential Equations: Periodic Solutions and Applications (Monographs and Surveys in Pure and Applied Mathematics)*. Chapman and Hall/CRC, 1993.
- [4] Olivier A. Bauchau and André Laulusa. Review of contemporary approaches for constraint enforcement in multibody systems. *Journal of Computational and Nonlinear Dynamics*, 3(1), 2008.
- [5] Dimitri P. Bertsekas. Projected newton methods for optimization problems with simple constraints. *SIAM Journal on Control and Optimization*, 20(2):221–246, mar 1982.
- [6] G. Bessonnet, P. Seguin, and P. Sardain. A parametric optimization approach to walking pattern synthesis. *The International Journal of Robotics Research*, 24(7):523–536, Jul 2005.
- [7] John T. Betts. *Practical Methods for Optimal Control and Estimation Using Non-linear Programming*. Society for Industrial & Applied Mathematics (SIAM), second edition, Jan 2010.
- [8] Pranav A. Bhounsule, Jason Cortell, Anoop Grewal, Bram Hendriksen, J. G. Daniël Karszen, Chandana Paul, and Andy Ruina. Low-bandwidth reflex-based control for lower power walking: 65 km on a single battery charge. *The International Journal of Robotics Research*, 33(10):1305–1321, Sep 2014.
- [9] Boston Dynamics. Atlas - The Agile Anthropomorphic Robot. http://www.bostondynamics.com/robot_Atlas.html, 2013. Last accessed 12/4/14.

- [10] Timothy C. Bretl and Stephen Rock. Planning robust dynamic transitions for enhanced mobility of planetary rovers. In *Proceedings of the 2nd IFAC Conference on Mechatronic Systems*, pages 109–114, Berkeley, CA, December 2002.
- [11] F. Bullo and M. Zefran. Modeling and controllability for a class of hybrid mechanical systems. *IEEE Trans. Robotics & Automation*, 18(4):563–573, 2002.
- [12] Anindya Chatterjee and Mariano Garcia. Small slope implies low speed for mcgeer’s passive walking machines. *Dynamics and Stability of Systems*, 15(2):139–157, 2000.
- [13] Vanessa E Hsu Chen. Passive dynamic walking with knees: A point foot model. Master’s thesis, Massachusetts Institute of Technology, 2007.
- [14] C. Chevallereau, G. Abba, Y. Aoustin, F. Plestan, E. R. Westervelt, C. Canudas-de-Wit, and J. W. Grizzle. Rabbit: A testbed for advanced control theory. *IEEE Control Systems Magazine*, 23(5):57–79, 2003.
- [15] C. Chevallereau, J. W. Grizzle, and C. Shih. Asymptotically stable walking of a five-link underactuated 3D bipedal robot. *IEEE Trans. Robotics*, 25(1):37–50, 2008.
- [16] J. C. Chiou and S. D. Wu. Constraint violation stabilization using input-output feedback linearization in multibody dynamic analysis. *Journal of Guidance, Control, and Dynamics*, 21(2):222–228, Mar 1998.
- [17] Howie Choset, Kevin M. Lynch, Seth Hutchinson, George A. Kantor, Wolfram Burgard, Lydia E. Kavraki, and Sebastian Thrun. *Principles of Robot Motion: Theory, Algorithms, and Implementations*. MIT Press, Cambridge, MA, June 2005.
- [18] S. H. Collins and A. L. Ruina. A bipedal walking robot with efficient and human-like gait. In *IEEE Int. Conf. on Robotics and Automation*, pages 1983–1988, Barcelona, Spain, 2005.
- [19] R Dumas, L Cheze, and J-P Verriest. Adjustments to mcconville et al. and young et al. body segment inertial parameters. *Journal of biomechanics*, 40(3):543–553, 2007.
- [20] Roy Featherstone. *Rigid Body Dynamics Algorithms*. Springer, 2007.
- [21] T. Fukuda, M. Doi, Y. Hasegawa, and H. Kajima. Multi-locomotion control of biped locomotion and brachiation robot. In *Fast Motions in Biomechanics and Robotics*, Lecture Notes in Control and Information Sciences, pages 121–145. Springer, Heidelberg, Allemagne, Germany, 2006.

- [22] M. Garcia, A. Chatterjee, A. Ruina, and M. Coleman. The simplest walking model: Stability, complexity, and scaling. *ASME J. Biomechanical Engineering*, 120(2):281–288, 1998.
- [23] Mariano Garcia, Anindya Chatterjee, and Andy Ruina. Efficiency, speed, and scaling of two-dimensional passive-dynamic walking. *Dynamics and Stability of Systems*, 15(2):75–99, Jun 2000.
- [24] Philip E. Gill, Walter Murray, and Michael A. Saunders. Snopt: An sqp algorithm for large-scale constrained optimization. *SIAM Journal on Optimization*, 12(4):979–1006, Jan 2002.
- [25] M. W. Gomes and A. L. Ruina. A five-link 2D brachiating ape model with life-like zero-energy-cost motions. *J. Theoretical Biology*, 237:265–278, 2005.
- [26] A. Goswami, B. Thuilot, and B. Espiau. A study of the passive gait of a compass-like biped robot: Symmetry and Chaos. *Int. J. Robotics Research*, 17(12):1282–1301, 1998.
- [27] R. D. Gregg, T. W. Bretl, and M. W. Spong. Asymptotically stable gait primitives for planning dynamic bipedal locomotion in three dimensions. In *IEEE Int. Conf. on Robotics and Automation*, pages 1695–1702, Anchorage, AK, 2010.
- [28] R. D. Gregg and M. W. Spong. Reduction-based control of three-dimensional bipedal walking robots. *Int. J. Robotics Research*, 26(6):680–702, 2010.
- [29] Robert D. Gregg, Adam K. Tilton, Salvatore Candido, Timothy Bretl, and Mark W. Spong. Control and planning of 3-d dynamic walking with asymptotically stable gait primitives. *IEEE Transactions on Robotics*, 28(6):1415–1423, dec 2012.
- [30] Brent Griffin. Nhvc3dsim_bag160728.zip. http://www.griffb.com/s/NHVC3DSim_BAG160728.zip, 2016.
- [31] Brent Griffin and Jessy Grizzle. Nonholonomic virtual constraints for dynamic walking. *2015 54th IEEE Conference on Decision and Control (CDC)*, Dec 2015.
- [32] Jessy W. Grizzle, Christine Chevallereau, Ryan W. Sinnet, and Aaron D. Ames. Models, feedback control, and open problems of 3D bipedal robotic walking. *Automatica*, 50(8):1955–1988, Aug 2014.
- [33] Kaveh Akbari Hamed, Brian G. Buss, and Jessy W. Grizzle. Exponentially stabilizing continuous-time controllers for periodic orbits of hybrid systems: Application

- to bipedal locomotion with ground height variations. *The International Journal of Robotics Research*, 35(8):977–999, Jul 2016.
- [34] Michael E. Henderson. Multiple parameter continuation: Computing implicitly defined k-manifolds. *International Journal of Bifurcation and Chaos*, 12(03):451–476, mar 2002.
- [35] Ayonga Hereid, Eric A. Cousineau, Christian M. Hubicki, and Aaron D. Ames. 3D dynamic walking with underactuated humanoid robots: A direct collocation framework for optimizing hybrid zero dynamics. *2016 IEEE International Conference on Robotics and Automation (ICRA)*, May 2016.
- [36] Ayonga Hereid, Christian M. Hubicki, Eric A. Cousineau, and Aaron D. Ames. Dynamic humanoid locomotion: A scalable formulation for HZD gait optimization. *IEEE Transactions on Robotics*, 34(2):370–387, apr 2018.
- [37] Christian Hubicki, Jesse Grimes, Mikhail Jones, Daniel Renjewski, Alexander Spröwitz, Andy Abate, and Jonathan Hurst. Atrias: Design and validation of a tether-free 3d-capable spring-mass bipedal robot. *The International Journal of Robotics Research*, 35(12):1497–1521, 2016.
- [38] F. Iida and R. Tedrake. Minimalistic control of a compass gait robot in rough terrain. In *IEEE International Conference on Robotics and Automation*, pages 1985–1990, May 2009.
- [39] Herbert B. Keller. Global homotopies and newton methods. *Recent Advances in Numerical Analysis*, pages 73–94, 1978.
- [40] C.T. Kelley. *Iterative Methods For Optimization*. Society for Industrial and Applied Mathematics, 1999.
- [41] B. Krauskopf, H.M. Osinga, and J. Galan-Vioque. *Numerical Continuation Methods for Dynamical Systems: Path Following and Boundary Value Problems*. Springer, 2007.
- [42] Yuri A. Kuznetsov. Elements of applied bifurcation theory. *Applied Mathematical Sciences*, 2004.
- [43] Pedro X. Miranda La Hera, Anton S. Shiriaev, Leonid B. Freidovich, Uwe Mettin, and Sergey V. Gusev. Stable walking gaits for a three-link planar biped robot with one actuator. *IEEE Transactions on Robotics*, 29(3):589–601, Jun 2013.

- [44] Chenggang Liu, Christopher G. Atkeson, and Jianbo Su. Biped walking control using a trajectory library. *Robotica*, 31(2):311–322, May 2012.
- [45] Guanfeng Liu and Zexiang Li. A unified geometric approach to modeling and control of constrained mechanical systems. *IEEE Transactions on Robotics and Automation*, 18(4):574–587, August 2002.
- [46] Libin Liu, KangKang Yin, Michiel van de Panne, and Baining Guo. Terrain runner: Control, parameterization, composition, and planning for highly dynamic motions. *ACM Trans. Graph.*, 31(6):154:1–154:10, November 2012.
- [47] A. W. Long, T. D. Murphey, and K. M. Lynch. Optimal motion planning for a class of hybrid dynamical systems with impacts. In *IEEE Int. Conf. Robotics & Automation*, pages 4220–4226, 2011.
- [48] Zhiguo Lu, Tadayoshi Aoyama, Kosuke Sekiyama, Yasuhisa Hasegawa, and Toshio Fukuda. Motion transfer control from walking to brachiation through vertical ladder climbing for a multi-locomotion robot. *IEEE/ASME Transactions on Mechatronics*, 19(5):1681–1693, 2014.
- [49] Anne E. Martin, David C. Post, and James P. Schmiedeler. Design and experimental implementation of a hybrid zero dynamics-based controller for planar bipeds with curved feet. *International Journal of Robotics Research*, 33(7):988–1005, 2014.
- [50] A. Mazumdar and H. H. Asada. An underactuated, magnetic-foot robot for steel bridge inspection. *ASME J. Mechanisms & Robotics*, 2(3), 2010.
- [51] T. McGeer. Passive dynamic walking. *Int. J. Robotics Research*, 9(2):62–82, 1990.
- [52] K. D. Mombaur, R. W. Longman, H. G. Bock, and J. P. Schloder. Open-loop stable running. *Robotica*, 23(1):21–33, January 2005.
- [53] Mohamad Shafiee Motahar, Sushant Veer, and Ioannis Poulakakis. Composing limit cycles for motion planning of 3d bipedal walkers. In *2016 IEEE 55th Conference on Decision and Control (CDC)*. IEEE, dec 2016.
- [54] J. Nakanishi, T. Fukuda, and D.E. Koditschek. A brachiating robot controller. *IEEE Trans. Robotics & Automation*, 16(2):109–123, 2000.
- [55] Jun Nakanishi, Andreea Radulescu, and Sethu Vijayakumar. Spatio-temporal optimization of multi-phase movements: Dealing with contacts and switching dynamics. In *IEEE Int. Conf. on Intelligent Robots and Systems*, pages 3108–3113, November 2013.

- [56] J. Nocedal and S. J. Wright. *Numerical Optimization*. Springer Verlag, 1999.
- [57] Open Source Robotics Foundation. `drc_skeleton_v3_mod1.cfg`. DARPA Robotics Challenge Simulator, default branch commit `dfb3482`, June 2014.
- [58] Michael Posa, Scott Kuindersma, and Russ Tedrake. Optimization and stabilization of trajectories for constrained dynamical systems. In *Proceedings of the International Conference on Robotics and Automation (ICRA)*, May 2016.
- [59] William H. Press, Saul A. Teukolsky, William T. Vetterling, and Brian P. Flannery. *Numerical Recipes in C: The Art of Scientific Computing*. Cambridge University Press, 2nd edition, 2002.
- [60] Andrew N. Pressley. *Elementary Differential Geometry*. Springer-Verlag, 2 edition, 2010.
- [61] W. R. Provancher, S. I. Jensen-Segal, and M. A. Fehlbeg. ROCR: An energy-efficient dynamic wall-climbing robot. *IEEE/ASME Trans. Mechatronics*, 16(5):897–906, 2011.
- [62] Alireza Ramezani, Jonathan W. Hurst, Kaveh Akbari Hamed, and J. W. Grizzle. Performance analysis and feedback control of atrias, a three-dimensional bipedal robot. *Journal of Dynamic Systems, Measurement, and Control*, 136(2):021012, Dec 2013.
- [63] Werner C. Rheinboldt. Numerical continuation methods: a perspective. *Journal of Computational and Applied Mathematics*, 124(1-2):229–244, Dec 2000.
- [64] F. Rochat, P. Schoeneich, M. Bonani, S. Magnenat, F. Mondada, and H. Blueler. Design of magnetic switchable device (MSD) and applications in climbing robot. In *CLAWAR*, 2010.
- [65] N. Rosa and K.M. Lynch. The passive dynamics of walking and brachiating robots: Results on the topology and stability of passive gaits. In *Nature-Inspired Mobile Robotics: Proceedings of the 16th International Conference on Climbing and Walking Robots and the Support Technologies for Mobile Machines*, 2013.
- [66] Nelson Rosa. Neuroscience and Robotics Lab GitHub page. <https://github.com/nxrllab/continuation>, 2014. Last accessed 1/17/16.
- [67] Nelson Rosa, Adam Barber, Robert D. Gregg, and Kevin M. Lynch. *Stable open-loop brachiation on a vertical wall*, pages 1193–1199. Institute of Electrical and Electronics Engineers, May 2012.

- [68] Nelson Rosa and Kevin M. Lynch. Extending equilibria to periodic orbits for walkers using continuation methods. *2014 IEEE/RSJ International Conference on Intelligent Robots and Systems*, Sep 2014.
- [69] Nelson Rosa and Kevin M Lynch. Using equilibria and virtual holonomic constraints to generate families of walking gaits. In *Dynamic Walking Conference*, Mariehamn, Finland, June 2017.
- [70] Cenk Oguz Saglam and Katie Byl. Robust policies via meshing for metastable rough terrain walking. In *Proceedings of Robotics: Science and Systems*, Berkeley, USA, July 2014.
- [71] Cenk Oguz Saglam and Katie Byl. Meshing hybrid zero dynamics for rough terrain walking. In *IEEE International Conference on Robotics and Automation*. IEEE, May 2015.
- [72] F. Saito, T. Fukuda, and F. Arai. Swing and locomotion control for a two-link brachiation robot. *IEEE Control Systems Magazine*, 14(1):5–12, 1994.
- [73] Steve Smale. A convergent process of price adjustment and global newton methods. *Journal of Mathematical Economics*, 3(2):107–120, Jul 1976.
- [74] Michael Spivak. *Calculus on Manifolds. A modern approach to classical theorems of advanced calculus*. W. A. Benjamin, Inc., New York-Amsterdam, 1965.
- [75] M. W. Spong. The swing up control problem for the Acrobot. *IEEE Control Systems Magazine*, 15(1):49–55, 1995.
- [76] M. W. Spong and F. Bullo. Controlled symmetries and passive walking. *IEEE Trans. Automatic Control*, 50(7):1025–1031, 2005.
- [77] K. Sreenath, H. W. Park, I. Poulakakis, and J. W. Grizzle. A compliant hybrid zero dynamics controller for stable, efficient and fast bipedal walking on MABEL. *Int. J. Robotics Research*, 2010.
- [78] Eric R Westervelt, Jessy W Grizzle, Christine Chevallereau, Jun Ho Choi, and Benjamin Morris. *Feedback control of dynamic bipedal robot locomotion*. CRC press Boca Raton, 2007.
- [79] W. Xi, Y. Yesilevskiy, and C. D. Remy. Selecting gaits for economical locomotion of legged robots. *The International Journal of Robotics Research*, Nov 2015.